energies

MDPI

Article

Optimal Voltage–Frequency Regulation in Distributed Sustainable Energy-Based Hybrid Microgrids with Integrated Resource Planning

Amar Kumar Barik [1], Dulal Chandra Das [1,*], Abdul Latif [1], S. M. Suhail Hussain [2] and Taha Selim Ustun [2]

[1] Department of Electrical Engineering, National Institute of Technology Silchar, Assam 788010, India; amar_rs@ee.nits.ac.in (A.K.B.); abdul_rs@ee.nits.ac.in (A.L.)
[2] Fukushima Renewable Energy Institute, AIST (FREA), National Institute of Advanced Industrial Science and Technology (AIST), Koriyama 963-0298, Japan; suhail@ieee.org (S.M.S.H.); ustun@ieee.org (T.S.U.)
* Correspondence: dulal@ee.nits.ac.in

Abstract: This work is the earliest attempt to propose an integrated resource planning for distributed hybrid microgrids considering virtual-inertia support (VIS) and demand-response support (DRS) systems. Initially, three-distributed sustainable energy-based unequal hybrid microgrids are envisioned with the availability of solar/wind/bioenergy resources. In order to overcome the effects of intermittency in renewable resources and low inertia, each microgrid is incorporated with DRS and VIS units for demand- and supply-side management, respectively. The proposed system is simulated in MATLAB considering real-time recorded solar/wind data with realistic loading for 12 months. A novel quasi-oppositional chaotic selfish-herd optimization (QCSHO) algorithm is proposed by hybridizing quasi-opposition-based learning and chaotic linear search techniques into the selfish-herd optimization, for optimal regulation of voltage and frequency in microgrids. Then, the system responses are compared with 7 algorithms and 5 error functions to tune PID controllers' gains, which confirmed the superiority of QCSHO over others. Then, the study proceeds to investigate the voltage, frequency, and tie-line power coordination in 5 extreme scenarios of source and load variations in the proposed system without retuning the controllers. Finally, the system responses are analyzed for 10 different possible allocation of VIS and DRS units in different microgrids to find the most suitable combinations, and the results are recorded.

Keywords: bio-energy generators; demand response; hybrid microgrids; integrated resource planning; optimization techniques; sustainable energy; virtual inertia

Citation: Barik, A.K.; Das, D.C.; Latif, A.; Hussain, S.M.S.; Ustun, T.S. Optimal Voltage–Frequency Regulation in Distributed Sustainable Energy-Based Hybrid Microgrids with Integrated Resource Planning. *Energies* **2021**, *14*, 2735. https://doi.org/10.3390/en14102735

Academic Editor: Mojgan Hojabri

Received: 5 April 2021
Accepted: 7 May 2021
Published: 11 May 2021

1. Introduction

The mounting global demand of electric power and depleting fossil resources for conventional generation are hammering to hunt the alternative source of sustainable energy. However, the most promising sustainable resources such as solar and wind are intermittent in nature with weather dependency, and the harnessed power from single source with available technology is too small to meet the demand. Hence, multi-resource-based sustainable generators are incorporated in local hybrid microgrids to improve reliability by coordinated generation [1]. The energy management in interconnected multi-microgrids are probed in [2]. The future power demand could be met by interconnecting such microgrids including locally available waste-to-energy-based bioenergy generator system (BEGS) along with solar/wind-based renewable energy systems (RES). The community waste could be collected, segregated, and preprocessed for power generation with suitable BEGS such as Biodiesel engine generator (BDEG) unit, Biogas turbine generator (BGTG) unit, waste-water-driven micro-hydro turbine generator (MHTG) unit, and biomass fired combined heat and power (BCHP) unit to support the RES units such as solar photovoltaic (SPV) arrays, solar thermal power (STP) plants, and wind turbine generator (WTG) units [1].

Conversely, these microgrids comprising small capacity renewable generators, have low inertia to handle larger load variations as well as renewable penetrations [3]. The change in consumer lifestyle with sophisticated electronic appliances/devices have also influenced the pattern of demand variation in recent days. Hence, it crafts a great challenge to supply quality power with adequate inertia support to microgrids involving intermittent renewable resources whose power generations are climate dependent.

Recent works have reported several methods to handle similar challenges. The adjustable [4] and derivative [5–7] technique-based virtual inertia control units are considered with supercapacitors [4–6] and super-magnetic energy storage [7] for frequency regulation of microgrids. The detail overview of virtual synchronous generators integrated to microgrids and power grids are discussed in [3] with their applications. A fast-acting inverter and storage-based VSG is developed to damp the oscillation of a DG in [8]. An extended virtual synchronous generator is proposed for load frequency control (LFC) of microgrids [9]. The inertia of AC microgrid with renewable penetrations is estimated by frequency response measurement using curve-fitting method in [10]. Most of the similar literature have designed VSG with energy storage system (ESS) and fast-acting bidirectional converter to improve the inertia and damping effect of microgrids. This motivates to propose a virtual inertia support (VIS) system with suitable ESS for supply-side management (SSM)-based IRP in distributed microgrids as illustrated in Figure 1 [11].

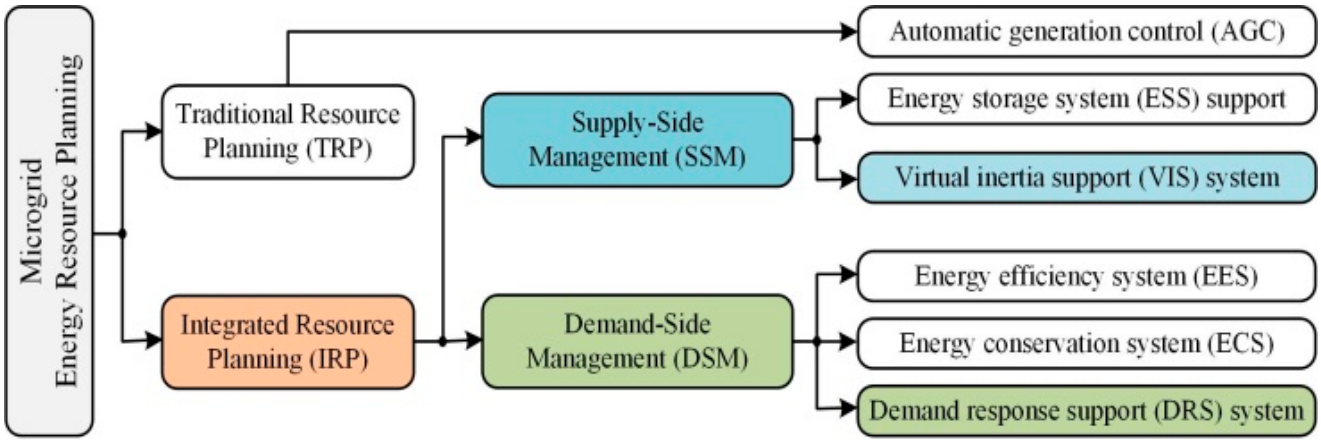

Figure 1. Energy resource planning in microgrids.

Similarly, the intermittency of RES units in microgrids could be managed by temporarily shifting their power consumptions with combination of some non-essential loads such as hybrid electric vehicles (HEV), heat pumps, water heaters, and freezers contributing the demand responses focused on demand-side management (DSM) [12]. The frequency regulation of multi-area power systems using demand response strategies are discussed in [13]. The emergency DSM program-based real-time voltage regulation is reported in [14]. The regulation of frequency in microgram with minimum manipulated loading proposing extensive central DSM algorithm is reported [15]. DSM strategies considering storage system [16] and HEV charging stations are successfully applied in isolated and interconnected microgrids [17,18]. This motivates to propose a demand response support (DRS) system with suitable DR strategy for DSM-based IRP in distributed microgrids as shown in Figure 1 [11]. Hence, there is a scope to design and allocate suitable VIS/DRS system for optimal regulation of voltage and frequency in distributed microgrids as very few/no works have been reported so far.

The power quality of microgrids could be improved by regulating the system voltage and frequency simultaneously incorporating automatic voltage regulator (AVR) along with automatic load-frequency control (ALFC) in isolated microgrid [1] and in distributed system [19]. The RES such as WTG, SPV, and linear Fresnel reflector (LFR) type STP units are integrated with waste-to-energy-based BEGS such as BDEG, BGTG, MHTG, and BCHP

units in this microgrid [1]. Some works applied battery energy storage (BES) units for ALFC of isolated [20] and interconnected [21,22] microgrids.

Most of the recent works on ALFC of microgrids claimed the efficacy of classical proportional-integral-derivative (PID) controllers over conventional integral (I), proportional-integral (PI), proportional-derivative (PD), and integral-derivative (ID) controllers [17–21]. Some modern controllers such as model predictive controller [19], fuzzy controller [22], fractional order controllers, and their blends [23,24] were also applied in similar works, however, they were corroborated with PID controllers. The effective tuning of these controllers in ALFC of these complex microgrids is achieved by applying some basic optimization algorithms such as: particle swarm optimization (PSO) [18], grasshopper optimization algorithm (GOA) [20,21], salp swarm algorithm (SSA) [25], selfish-herd optimization (SHO) [26], or their hybrids such as quasi-oppositional selfish-herd optimization (QSHO) [1,17]. Likewise, the quasi-oppositional chaotic antlion optimizer algorithm is projected in [27] by hybridizing quasi-opposition-based learning (QOBL) and chaotic linear search (CLS) techniques with antlion optimization. Inspiringly, a novel algorithm named "quasi-oppositional chaotic selfish-herd optimization" (QCSHO) is proposed here for tuning the PID controllers by hybridizing QOBL and CLS techniques [27] with the basic SHO [28] algorithm to replicate the chaotic behavior of the selfish herds.

Encouraged with all these recent literatures and their scopes, this work has proposed a combined SSM-/DSM-based IRP for 3 unequal interconnected microgrids considering the limitations on availability/accessibility of different resources to replicate dispersed generation (DG), where, each of the microgrids is encompassed with a distinct RES-BGES unit pair to supply the tentative demand including BDEG unit as backup support and VIS/DRS unit for system stability. The system performances are analyzed using the proposed QCSHO tuned PID controllers in 5 different scenarios of extreme source/load variations, designing the linearized Simulink model of distributed microgrids. The nomenclature and design values of system parameters considered in this work are listed in Table 1. The key contributions are:

(a) Proposing IRP for simultaneous voltage–frequency regulation of multi-unit-based distributed microgrids by designing combined storage-based VIS system for SSM and HEV charging station-based DRS for DSM.
(b) Designing a novel QCSHO algorithm by hybridizing CLS and QOBL with basic SHO algorithms to tune the PID controller gains, introducing integral-square of weighted absolute error (ISWAE) for interconnected microgrids.
(c) Analyzing the system responses with the proposed VIS/DRS units considering random linear/non-linear loadings for exact replication of real-time load patterns including recorded wind/solar data to check the reliability of the distributed microgrids round the year.
(d) Investigating the optimal allocation of VIS/DRS units for economic operation of distributed microgrids.

Table 1. Nomenclature used in this work.

Symbol	Nomenclature	Values
Δf_i	Frequency deviation (Hz) of ith microgrid.	
Δu_i	Voltage deviation (volt) of ith microgrid.	
ΔP_{tii}	Net tie-line loading on ith microgrid.	
D_i	Load damping coefficient of ith microgrid.	0.014, 0.012, 0.010
M_i	Mutual inertia coefficient of ith microgrid.	0.24, 0.22, 0.20
R_i	Droop coefficient of ith microgrid.	2.0
B_i	Frequency biasing factor of ith microgrid.	0.514, 0.512, 0.510

Table 1. *Cont.*

Symbol	Nomenclature	Values
T_{ij}	Coefficient for synchronizing torque.	0.080
a_{12}, a_{23}, a_{31}	Inter-grid power transfer ratios	$-6/5$, $-5/4$, $-4/6$
T_1, T_2, T_3, T_4,	lead/lag switching delays of converter in VIS system	0.279 s, 0.026 s, 0.411 s, 0.1 s
K_{BES}, T_{BES}	Gain and time constant of BES unit.	0.003, 0.1 s,
K_{CES}, T_{CES}	Gain and time constant of CES unit.	0.07, 0.9 s,
K_{HEV}, T_{HEV}	Gain and time constant of HEV unit	1, 0.02 s
K_{LFR}, T_{LFR}, K_{ORC}, T_{HX}, T_{ST}	Gain and time constants of LFR, heat-exchanger and turbine of STP unit.	5.0, 0.42 s, 0.95, 0.1 s, 0.3 s
T_{PV}, T_{WT}	Time constant of SPV and WTG units.	1.8 s, 1.5 s
T_{CR}, T_{BG}, X_c, Y_c, b_B, T_{BT}	Combustion reaction delay, biogas delay, lead time, lag time, valve actuator and discharge delay of BGTG unit.	0.01 s, 0.23 s, 0.6,.0 s, 0.05 s, 0.2 s
T_{VA}, T_{BE}	Valve and engine delays of BDEG unit.	0.055 s, 0.5 s
T_{HG}, T_{RS}, T_{RH}, T_{HT}	Time constants of governor, reset, droop, and turbine of MHTG unit.	0.2 s, 5.0 s, 28.75 s, 1.0 s
T_{BCT}, T_{BSG}, T_R, K_R	Time constants of turbine, governor, and reheat with gain of BCHP unit.	0.08 s, 0.3 s, 0.3, 10 s
K_{BC}, K_{BG}, K_{MH}, K_{BD}, K_{BE}, K_{CE}	Participation factors of BCHP, BGTG, MHTG, BDEG, BES, and CES units.	0.25, 0.25, 0.25, 0.25, 0.5, 0.5
P_s, K_1, K_2, K_3, K_4	Coupling coefficients of AVR unit.	0.145, 0.2, -0.1, 0.5, 1.4,
K_A, T_A, K_E, T_E, K_S, T_S, K_F, T_F, K_C, T_C	Gain and delays of compensators, field, exciter, amplifier, and sensor of AVR unit.	40, 0.05 s, 1.0, 0.55 s, 1.0, 0.05 s, 0.8 s, 1.4 s, 0.5, 0.715 s
U_{SFi}, U_{SVi}, U_{STi}	Peak undershoots in Δf_i, Δu_i, and ΔP_{tii}	
O_{SFi}, O_{SVi}, O_{STi}	Peak overshoots in Δf_i, Δu_i, and ΔP_{tii}.	
T_{SFi}, T_{SVi}, T_{STi}	Settling-times of Δf_i, Δu_i, and ΔP_{tii}.	

The rest part of this work is organized as follows. The component-wise mathematical modelling of the proposed distributed microgrids is deliberated in Section 2. The projected QCSHO algorithm is illustrated with detailed steps in Section 3. The simulated results for all possible scenarios are discussed in Section 4, and Section 5 briefly concludes the work.

2. Modeling of Distributed Microgrid System

The entire work is investigated by proposing community-based autonomous microgrids with available sustainable resources of the locality and expected to use all the bio-waste of the locality for energy generation in suitable BEGS considering optimal usage of available RES as illustrated in Figure 2a [1]. However, all these resources may not be available in same place, thereby encouraging DG [16,20]. Hence, three-interconnected sustainable energy-based unequal microgrids are proposed here, comprising LFR type STP/BCHP/BDEG1 units in the first microgrid (hμG1), WTG/BGTG/BDEG2 units in the second microgrid (hμG2), and SPV/MHTG/BDEG3 units in the third microgrid (hμG3), with combined SSM-/DSM-based IRP as illustrated in Figure 2b. The linearized system model of the complete proposed microgrids is shown in Figure 3a. The prime objective of the work is to maintain the system voltage–frequency (440 v–50 Hz) within accessible limit irrespective of the RES penetration and load disparities. The component-wise linear model of this microgrids is concisely conferred in this section considering design values of parameters listed in Table 1 [1,17].

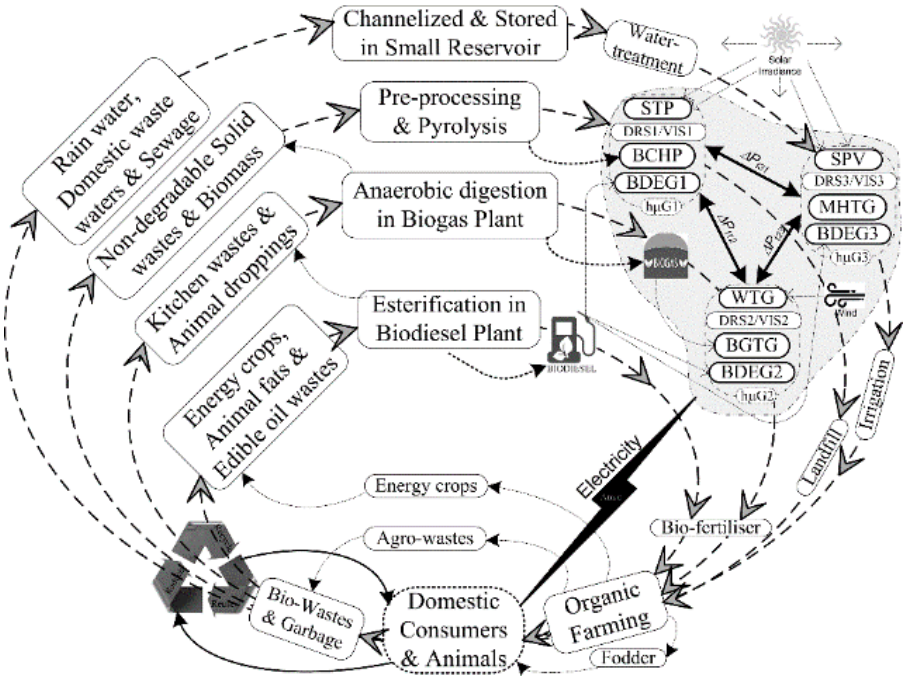

(**a**)

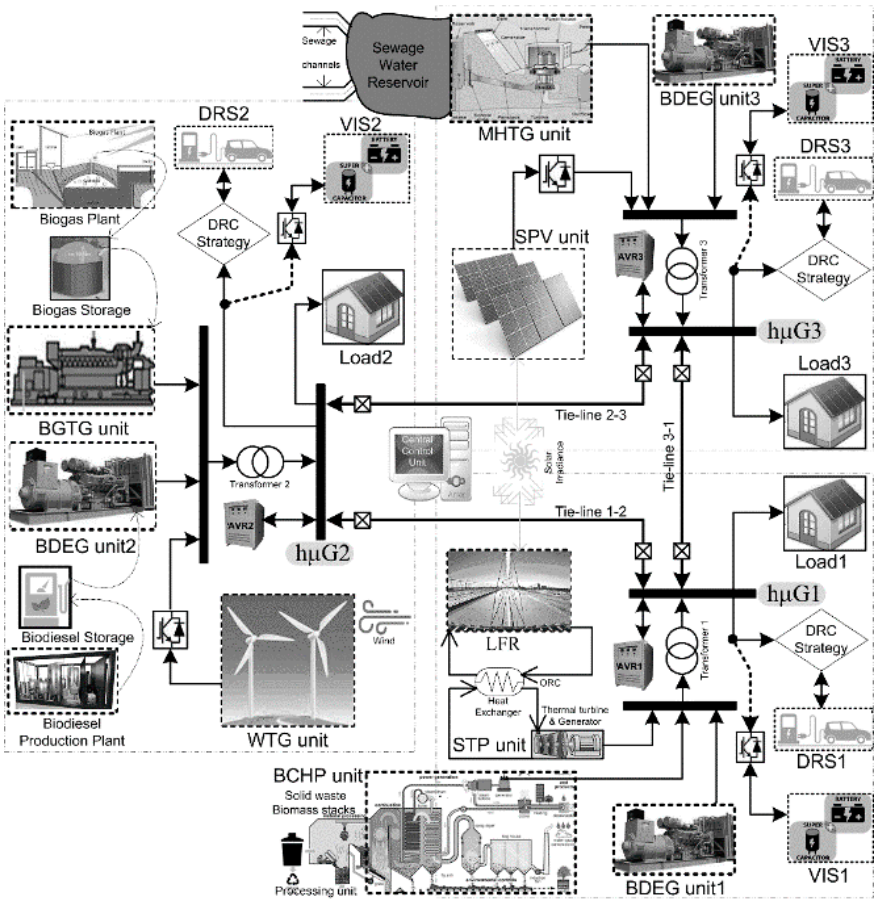

(**b**)

Figure 2. (**a**) Waste-to-energy cycle allied to distribution of microgrids and (**b**) schematics of the proposed interconnected microgrids.

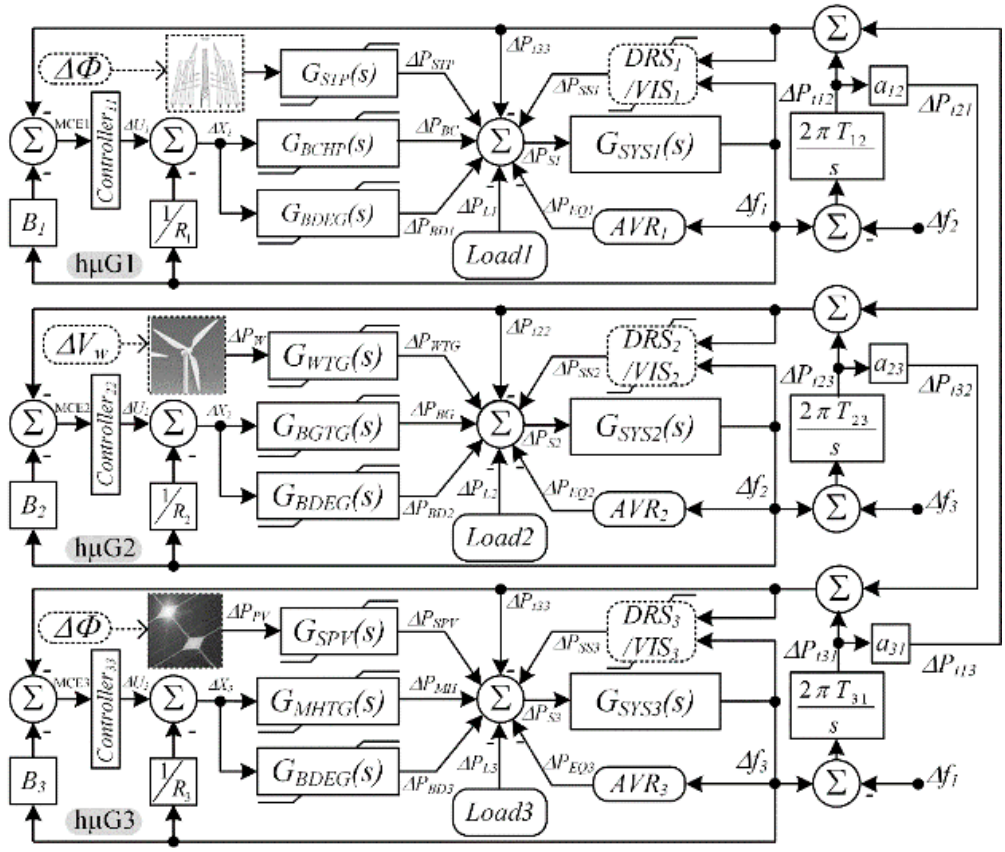

(**a**)

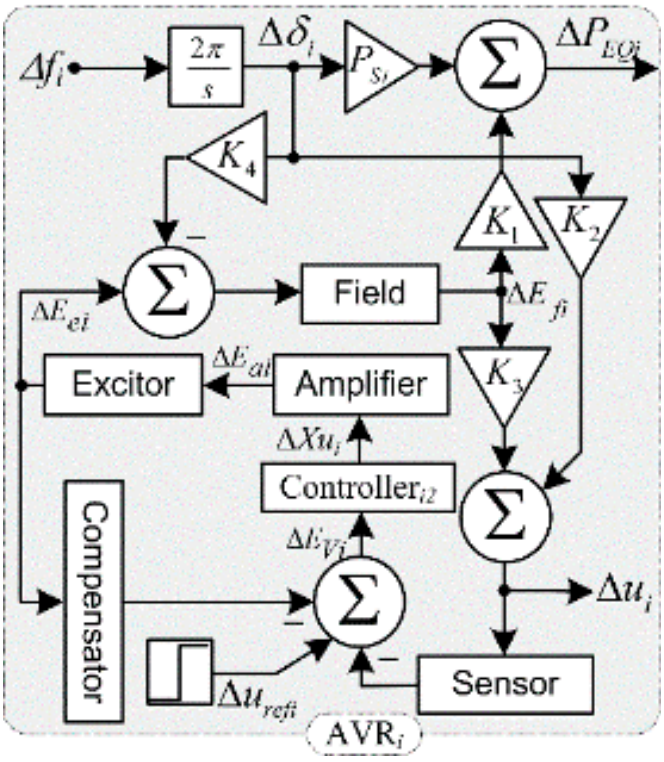

(**b**)

Figure 3. *Cont.*

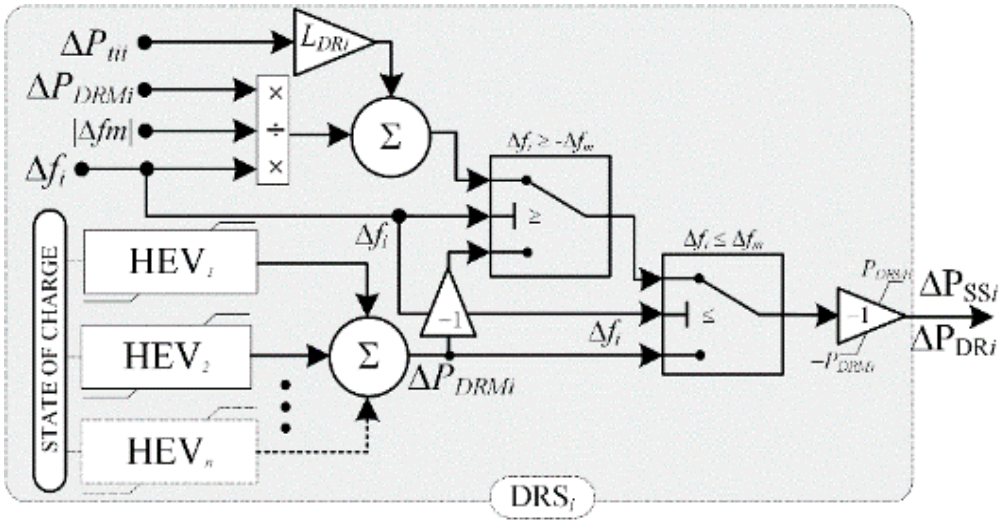

(**c**)

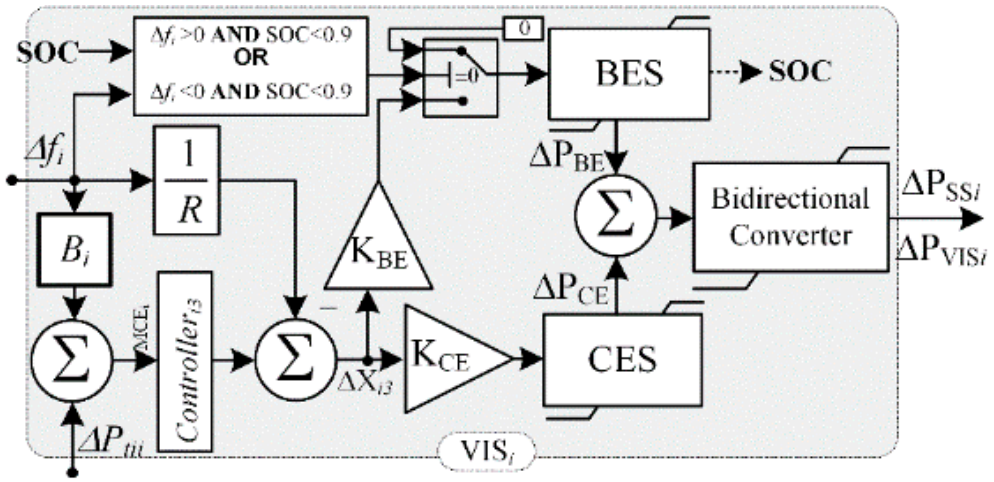

(**d**)

Figure 3. Simulink models: (**a**) interconnected microgrids, (**b**) model of AVR unit, (**c**) model of DRS unit, and (**d**) model of VIS unit.

2.1. Frequency Regulation System

The system frequency of each microgrid is regulated by ALFC unit combined of primary (droop) control and secondary (PID) control. The effect of ALFC with PID controllers (ΔX_{i1}) are expressed in (1) for *i*th microgrid and the effective tie-line power exchange on *i*th microgrid(ΔP_{tii}) considering frequency bias (B_i) is expressed in (2) (for $i = 1, 2, 3$) [29].

$$\Delta X_{i1} = (-B_i \Delta f_i - \Delta P_{tii}) \left(K_{Pi1} + \frac{K_{Ii1}}{s} + sK_{Di1} \right) - \frac{1}{R_i} \Delta f_i \tag{1}$$

$$\Delta P_{tii} = \sum_{\substack{j,i=1 \\ (j \neq i)}}^{3} \Delta P_{tij} = \sum_{\substack{j,i=1 \\ (j \neq i)}}^{3} (\Delta f_i - \Delta f_j) \frac{2\pi T_{ij}}{s}. \tag{2}$$

2.2. Voltage Regulation System

The system voltage of *i*th microgrid is regulated by dedicated AVR units as modelled in Figure 3b. The detailed modelling of AVR unit is discussed and successfully operated

in both isolated [1] and interconnected [19] microgrids. This work has employed separate PID controllers for each AVR units with control actions (ΔX_{i2}) assessed in (3). The power exchange (ΔP_{EQ}) for AVR and voltage variation (Δu_i) for ith microgrids are specified in (4)–(5), respectively [1].

$$\Delta X_{i2} = \left(K_{Pi2} + \frac{K_{Ii2}}{s} + sK_{Di2}\right)\Delta E_{Vi} \tag{3}$$

$$\Delta P_{EQi} = P_S \Delta\delta_i + K_1 \Delta E_{fi} \tag{4}$$

$$\Delta u_i = K_2 \Delta\delta_i + K_3 \Delta E_{fi}. \tag{5}$$

2.3. Virtual Inertia Support System

The larger load variations or higher renewable penetrations are mostly responsible for system frequency instability in autonomous microgrids due to small inertia [3,5]. Therefore, it is vital to provide inertia support to those microgrids, virtually [3–5] with suitable ESS and bidirectional power convertors considering SSM-based IRP. The inertia power (H) of the microgrid could be estimated by (6) considering apparent power $\hat{S}$, mechanical (T_m and P_m), and electrical (T_e and P_e) torques/powers measuring the system frequency ($\omega = 2\pi f$) [29].

$$\frac{d\omega}{dt} = \frac{\omega^2(T_m - T_e)}{2H\hat{S}} = \frac{\omega(P_m - P_e)}{2H\hat{S}}. \tag{6}$$

Hence, most of the recent works [5–7] were applied derivative technique-based virtual inertia control in accordance to (6) by estimating an inertia gain times derivative of measured frequency error (Δf), which replicates a derivative controller. However, the derivative controllers used alone will intensify the steady state error as well as the noise signals and cause saturation effects [29]. In order to overcome these issues, this work includes PI-controller parallel to derivative controller (combined to replicate the PID controller) to process Δf as modelled in Figure 3c.

Recent works have successfully used supercapacitors [4–6] and super-magnetic coils [7] as ESS in VIS. However, higher penetration of RES from WTG/SPV should be absorbed to counter their adverse effects on system frequency, using some storage units such as BES. Hence, this work proposes a new VIS unit including fast-switching bidirectional power converter as in Figure 3c, combining CES and BES units-based on their state-of-charge (SOC) conditions as shown in Figure 3c. The BES unit could store more power for longer durations depending on the stack size/capacity of the battery units and support the CES unit during higher RES penetration or load variations.

Separate PID controllers are dedicated with control actions (ΔX_{i3}) expressed as (7) for regulating each VIS unit of ith microgrids. The regulated power exchange (ΔP_{VISi}) in every VIS units could be estimated by its linearized model as (8) for ith microgrids, considering healthy battery conditions, i.e., 20% < SOC < 90% [26].

$$\Delta X_{i3} = (-B_i \Delta f_i - \Delta P_{tii})\left(K_{Pi3} + \frac{K_{Ii3}}{s} + sK_{Di3}\right) - \frac{1}{R_i}\Delta f_i \tag{7}$$

$$\Delta P_{VISi} = \left(\frac{K_{BE}K_{BES}}{1 + sT_{BES}} + \frac{K_{CE}K_{CES}}{1 + sT_{CES}}\right)\left(\frac{1 + sT_1}{1 + sT_2}\right)\left(\frac{1 + sT_3}{1 + sT_4}\right)\Delta X_{i3}. \tag{8}$$

2.4. Demand Response Support System

The combined demand response could afford smooth characteristics of frequency response by suitably managing the frequency threshold of every DRS devices associated to the microgrids. The HEV charging station of locality is considered as the DRS unit in this work for contract-based DSM as modelled in Figure 3d. Net power to be activated by each DRS unit of ith microgrid at any instance (ΔP_{DRi}) could be assessed by the strategy (9) [12,13] considering the change in maximum available DRS (ΔP_{DRMi}) in ith microgrids

estimated by (10) based on DRS contract with the charging station of HEV [17,18]. The range of maximum frequency regulation is decided by the utility, and this work considered, Δf_m = 0.05 Hz, where the tie-line loading coefficients (L_{DRi}) for DRS are proportional controller gains and tuned with optimization techniques [17,18].

$$\Delta P_{DRi} = \begin{cases} -\frac{\Delta f_i}{\Delta f_{\mathrm{m}}} \Delta P_{DRMi} - L_{DRi} \Delta P_{tii}, & -\Delta f_{\mathrm{m}} \le \Delta f_i \le \Delta f_{\mathrm{m}} \\ -\frac{\Delta f_i}{|\Delta f_i|} \Delta P_{DRMi}, & Otherwise \end{cases} \tag{9}$$

$$\Delta P_{DRMi} = \sum_{k=1}^{n} SOC_i^k \frac{K_{HEV}}{1 + sT_{HEV}}. \tag{10}$$

2.5. Renewable Energy System

The LFR type STP unit is preferred over parabolic trough collector type STP for lesser land requisition [17], whose power exchange is expressed as (11) with change in solar irradiance ($\Delta\Phi$) [1,17]. The power exchange of SPV unit due to change in $\Delta\Phi$ is stated in (12) with efficiency (η = 10%), temperature (Ta = 27.2 °C), and solar surface area (S = 4084 m^2) as testified in [30]. The power exchange of WTG unit owing to change in wind speed (ΔV_W) is articulated in (13) with air density (ρ = 1.25 kg/m^3) and blade-swept area (A_r = 1735 m^2), whose power coefficient (C_p) is assessed by (14) [30]. The net RES penetration of each microgrids is estimated as (15).

$$\Delta P_{STP} = \left(\frac{K_{LFR}}{1 + sT_{LFR}}\right)\left(\frac{K_{ORC}T_{HX}}{1 + sT_{Hx}}\right)\left(\frac{1}{1 + sT_{ST}}\right)\Delta\Phi \tag{11}$$

$$\Delta P_{SPV} = \frac{\eta S\{1 - 0.005(25 + T_a)\}}{1 + sT_{PV}}\Delta\Phi \tag{12}$$

$$\Delta P_{WTG} = \frac{0.5\rho C_p A_r V_W^3}{1 + sT_{WT}}\Delta V_W \tag{13}$$

$$100C_P = (44 - 1.67\beta)\sin\left(\frac{(\lambda - 3)\pi}{15 - 0.3\beta}\right) - 1.84(\lambda - 3)\beta \tag{14}$$

$$\Delta P_{RES1} = \Delta P_{STP};\ \Delta P_{RES2} = \Delta P_{WTG};\ \Delta P_{RES3} = \Delta P_{SPV}. \tag{15}$$

The monthly average wind/solar data of Bhubaneswar city (India), were collected from "NASA Surface meteorology and Solar Energy—Available Tables" [31] and considered in this work to study the system performance round the year as mentioned in Figure 4.

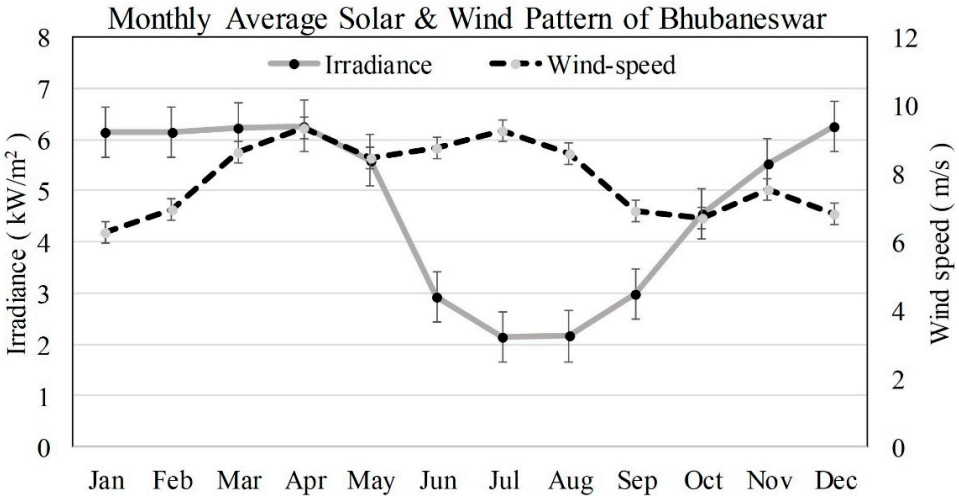

Figure 4. Monthly average solar/wind pattern of Bhubaneswar, India, used in this study.

2.6. Bioenergy Generator System

The community wastes (solid/liquid) are separately collected, segregated, and pre-processed to be ready for power generation in appropriate BEGS units (i.e., BCHP, BDEG, BGTG, and MHTG) and support the waste-to-energy-based microgrids [1]. The detail modelling of these units is discussed in [17,18], however, the respective power supplied by BCHP, BGTG, MHTG, and $BDEG_i$ units is expressed in (16)–(19), respectively [1]. In addition, the net contributions from each BEGS unit of ith microgrid are estimated as (20) (for i = 1, 2, 3).

$$\Delta P_{BC} = \left(\frac{K_{BC}}{1+sT_{BSG}}\right)\left(\frac{1+sK_RT_R}{1+sT_R}\right)\left(\frac{1}{1+sT_{BCT}}\right)\Delta X_{11} \tag{16}$$

$$\Delta P_{BG} = \left(\frac{1+sX_c}{(1+sY_c)(1+sb_B)}\right)\left(\frac{1+sT_{CR}}{1+sT_{BG}}\right)\left(\frac{K_{BG}}{1+sT_{BT}}\right)\Delta X_{21} \tag{17}$$

$$\Delta P_{MH} = \left(\frac{K_{MH}}{1+sT_{HG}}\right)\left(\frac{1+sT_{RS}}{1+sT_{RH}}\right)\left(\frac{1-sT_{HT}}{1+0.5sT_{HT}}\right)\Delta X_{31} \tag{18}$$

$$\Delta P_{BDi} = K_{BDi}\left(\frac{1}{1+sT_{VA}}\right)\left(\frac{1}{1+sT_{BE}}\right)\Delta X_{i1} \tag{19}$$

$$\Delta P_{BEG1} = \Delta P_{BC} + \Delta P_{BD1},\ \Delta P_{BEG2} = \Delta P_{BG} + \Delta P_{BD2},\ \text{and}\ \Delta P_{BEG3} = \Delta P_{MH} + \Delta P_{BD3} \tag{20}$$

2.7. Load-Generator Dynamic System

This work has used the monthly power consumption data of 3 consumers from different locations of Bhubaneswar in 2017 and normalized those to fit within the simulation time (t_{sim}) of the proposed microgrids as illustrated in Figures 5 and 6. So, the effective linear load (LL) deviation (ΔP_{LLi}) of ith microgrids in Figure 5 could be replicated for analyzing the system performances round the year, from this real data. However, the practical load pattern consists of nonlinearities injected collectively by several non-linear devices and power converters. Hence, this work has included an effective non-linear loading (NL) configuration (ΔP_{NL}) as (21) [1] for designing the net loading (ΔP_{Li}) as (22), equivalent to actual demand pattern of ith microgrids, as illustrated in Figure 6.

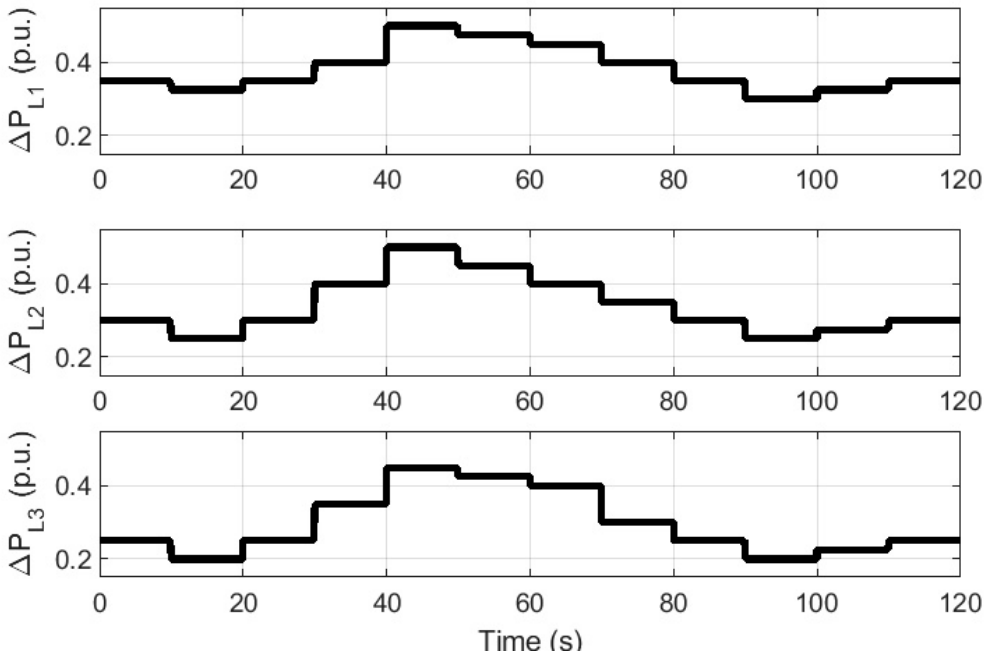

Figure 5. Loading pattern of 3 microgrids considering LL.

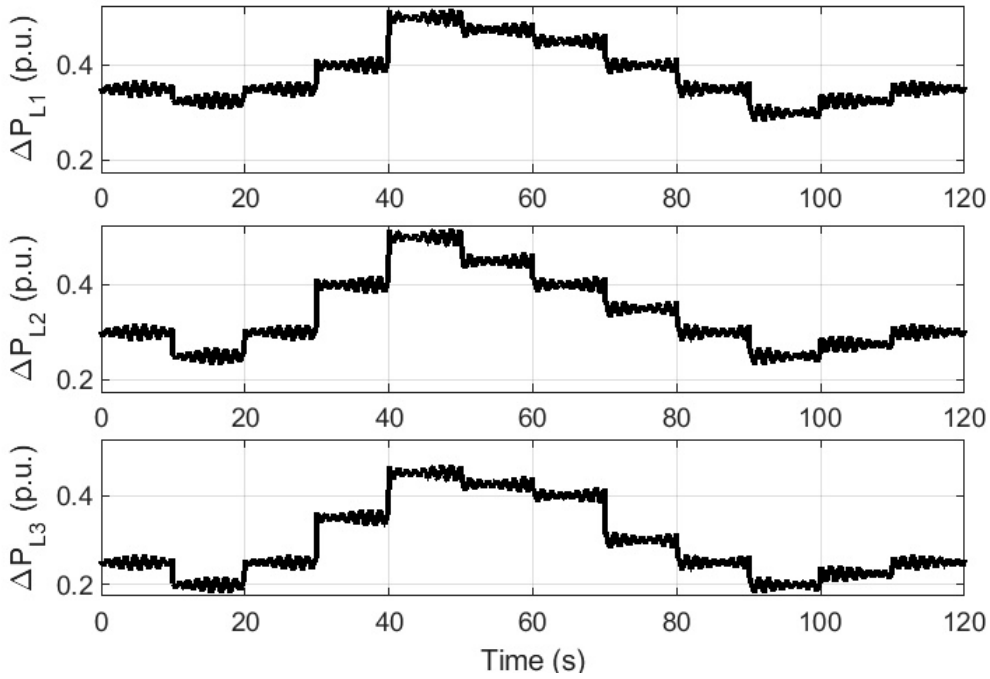

Figure 6. Loading pattern of 3 microgrids considering both LL and NL.

$$\Delta P_{NL} = (3\sin(36.942t) + 5\sin(4.417t) - 10\sin(5t)) \times 10^{-3} \tag{21}$$

$$\Delta P_{Li} = \Delta P_{LLi} + \Delta P_{NL}. \tag{22}$$

The effective load-generator dynamics for ith microgrids could be estimated as (23), considering single generator–load model [29] for low-inertia (H = 0.1 s) with 50 Hz nominal frequency. Here, the net instantaneous power error (ΔP_{Li}) of ith microgrids is estimated as (24) considering all source and loadings with VIS/DRS.

$$\Delta f_i = \frac{1}{D_i + sM_i} \Delta P_{Ei} \tag{23}$$

$$\Delta P_{Ei} = \Delta P_{RESi} + \Delta P_{BEGi} + \Delta P_{DRi} + \Delta P_{VISi} - \Delta P_{EQi} - \Delta P_{Li} - \Delta P_{tii}. \tag{24}$$

2.8. Objective Function Formulation

The system objective is estimated by the net deviation in apparent power considering corresponding weights for Δu and Δf as w_v and w_f. This could be implemented as the objective function (J), named "integral-square of weighted absolute error" (ISWAE) [1], which needs to be minimized for simultaneous reduction in system voltage, frequency, and tie-line loading. The exact objective for the proposed interconnected system could be expressed as (25), prioritizing frequency regulation (w_f = 1) than the voltage with a 10% slackening (w_v = 0.9) and relaxing tie-line loading 5% (w_t = 0.95).

$$\begin{aligned} Min. \quad & J = \int_0^{t_{sim}} \left\{ \sum_{i=1}^{3} \left[\left(w_f |\Delta f_i| \right)^2 + (w_v |\Delta u_i|)^2 + (w_t |\Delta P_{tii}|)^2 \right] \right\} dt \\ s. \quad t. \quad & lb \le K_{Cij} \le ub \end{aligned} . \tag{25}$$

Here, K_{Cij} denotes the PID gains (K_{Pij}, K_{Iij}, and K_{Dij}) for jth controller in ith microgrids, considering limits of lb and ub (lower and upper bounds).

The basic figures of demerits (FOD) [1], such as peak-overshoots, peak-undershoots, and settling-times for voltage, frequency, and tie-line loading of the proposed microgrids

are assessed with a 0.1% band. The performance index based on FOD (JFOD) of the distributed microgrids is estimated by (26) to investigate the overall system responses.

$$J_{FOD} = \sum_{i=1}^{3}\left(U_{SFi}^2 + O_{SFi}^2 + T_{SFi}^2 + U_{SVi}^2 + O_{SVi}^2 + T_{SVi}^2 + U_{STii}^2 + O_{STii}^2 + T_{STii}^2\right). \quad (26)$$

This work proposed a new QCSHO algorithm discussed in the next section for tuning all controller gains for minimizing the objective (J).

3. Quasi Oppositional Chaotic Selfish Herd Optimization

The selfish conduct of animals scavenging in herds, for survival during threat from predators was reported as SHO algorithm by Fausto et al. [28]. The movement of these selfish animals to acquire the central position with intraspecific competitions during predation for increasing their survival chance is articulated as SHO.

SHO algorithm is inspired from the predator/preys models, during predators' attack, which may influence a chaotic selfish-herd movement towards the center for survival. The expected competitions among selfish herds are very high in the chaos zone as illustrated in Figure 7a, enforcing a crowded movement near the center. However, the life-threats of animals facing the predators (H_{xi}, H_{xy}, and H_{xj}) are more compared to the conspecifics opposite (O_{xi}, O_{xy}, and O_{xj}) to them. Again, an animal with less competition (H^*_{xi}, H^*_{xy}, and H^*_{xj}) may be available in the quasi-opposite places instead of opposite points (O_{xi}, O_{xy}, and O_{xj}) concerning the center of the herd as demonstrated in Figure 7a. This idea inspired to modify SHO so as to replace the higher-risk chaotic animals (H^*_{xi}, H^*_{xy}, and H^*_{xj}) with the lower survival-risk individuals (H_{xi}, H_{xy}, and H_{xj}) during predation, for a better optimal solution. A new QCSHO algorithm is developed by hybridizing both the concepts of QOBL and CLS into the basic SHO algorithm to imitate this typical activity of selfish-herds during predation, considering a logistic map for CLS in (27), for a faster solution [27].

$$\begin{gathered} Ch_{i+1} = \mu(1 - Ch_i)Ch_i \\ \text{where, } Ch_i \in (0,1) \text{ and } Ch_i \neq 0.25,\ 0.5,\ 0.75 \end{gathered} \quad (27)$$

The central (M_{xy}) and opposite (O_{xy}) animal for a selected (H_{xy}) individual in the herd could be expressed by (28) considering maximum/minimum limit of the parameters. According to QOBL, the quasi-opposite animal in the herd is selected based on (29), comparing a random number (R_j) with the jumping rate.

$$M_{xy} = \left(ub_y + lb_y\right)/2, \text{ and } O_{xy} = ub_y + lb_y - H_{xy} \quad (28)$$

$$H^*_{xy} = \begin{cases} M_{xy} + \left(O_{xy} - M_{xy}\right).R_j, & \text{if } H_{xy} < M_{xy} \\ O_{xy} + \left(M_{xy} - O_{xy}\right).R_j, & \text{otherwise} \end{cases}. \quad (29)$$

The performance of SHO is expected to be improved by the modified QCSHO with the advantages of both CLS and QOBL that supports faster search process than normal stochastic search [27]. The detail steps of proposed QCSHO algorithm are illustrated as flowchart in Figure 7b with inclusions of both CLS and QOBL steps. The new QCSHO algorithm invokes the Simulink models of the system to evaluate/update the survival values of herds in each iteration as explained in Figure 7b, by passing the tuned controller gains and finding the optimal solution. The detailed simulation results and performance comparisons are discussed in the following section.

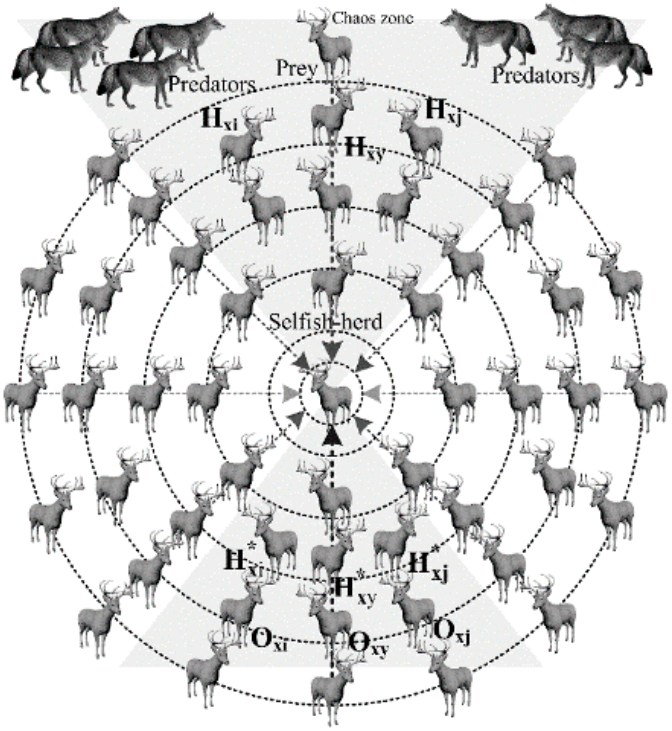

(**a**)

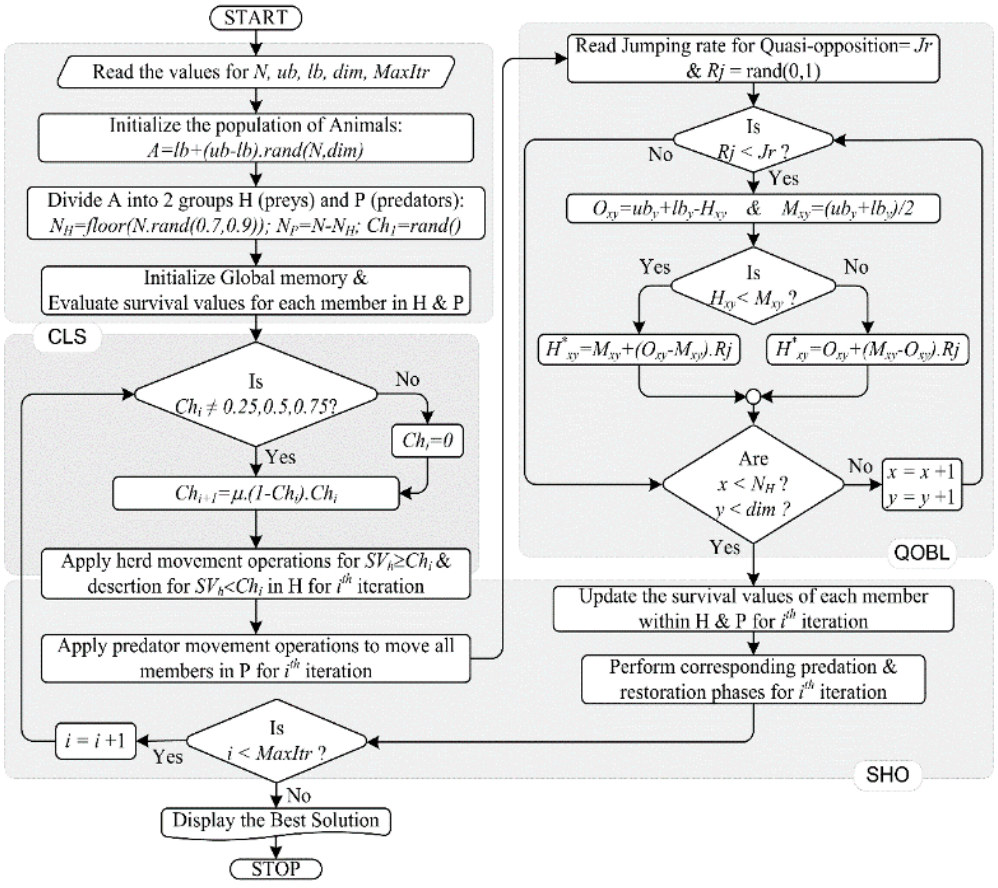

(**b**)

Figure 7. QCSHO algorithm: (**a**) chaotic herds' encircling and (**b**) flowchart.

4. Simulation Studies and Analysis of Results

The linear transfer-function model of the projected microgrids, illustrated in Figure 3a, is developed by Simulink® of MATLAB® R2015a software, whereas all the optimization algorithms are coded in script files. The performances of distributed microgrids were investigated for simultaneous voltage–frequency regulation by simulating with a desktop (4 GB RAM, Intel-3.4 GHz i7-4770 CPU) in following approaches.

4.1. Step Response Analysis for Method Selection

It is crucial to choose suitable methods such as optimization technique, objective function, and controllers for investigating the system responses commendably. The step responses of the proposed distributed microgrids are analyzed to compare these methods considering a step change in ΔP_L (drops to 0.725 from 0.75 p.u.), $\Delta\Phi$ (rises to 0.645 from 0.615 kW/m^2), and ΔV_w (rises to 6.96 from 6.3 m/s), for t_{sim} = 20 s with normal day scenario, in this subsection. Then, the superior methods are assorted to study the simultaneous voltage–frequency regulation in distributed microgrids with both VIS and DRS.

The proposed distributed microgrids in Figure 3a is simulated with PSO, GOA, SSA, SHO, QSHO, and CSHO and the projected QCSHO to minimize the objective functions J in (25). The important parameters for corresponding algorithms are recorded in Table 2.

Table 2. Key parameters for corresponding algorithms.

Algorithm	Specific Parameters	Common Parameters
PSO	c_1 = 1.5; c_2 = 2.0; w = 1; wd = 0.99	Population size, N = 50; Lower bound, lb = 0; Upper bund, ub = 20; Dimensions, dim = 30; Maximum iteration, $MaxItr$ = 100; Simulation time, t_{sim} = 20 s, 120 s.
GOA	C_{max} = 1; C_{min} = 4 × 10^{-5}; f = 0.5; L = 1.5	
SSA	C_2 = rand(); C_3 = rand()	
SHO	α, β, γ, δ = rand(); Prey_rate = [0.7, 0.9]	
QSHO	Jr = 0.25; Rj = rand()	
CSHO	Ch_1 = rand(); μ = 4.0	
QCSHO	μ = 4.0, Jr = 0.25; Rj = rand() = Ch_1;	

The convergence curves of all 7 optimization algorithms with step responses are compared in Figure 8, considering PID controllers with proposed ISWAE as (25) for initial 20 s of loadings. The FOD-based performance index (J_{FOD}) of the system expressed in (26) are estimated for all algorithms considering ISWAE and compared in the first column of Table 3. It is observed from Figure 8 and Table 3 that the proposed QCSHO performs superior over other algorithms.

Table 3. Comparison of objective functions using PID controllers.

J	ISWAE	IAE	ISE	ITAE	ITSE
PSO	0.382	1.396	0.042	7.190	0.182
GOA	0.319	1.167	0.035	6.010	0.152
SSA	z0.208	1.297	0.040	6.680	0.169
SHO	0.110	1.379	0.039	7.751	0.162
QSHO	0.091	1.426	0.043	7.343	0.185
CSHO	0.080	1.141	0.048	6.410	0.198
QCSHO	**0.012**	**1.076**	**0.020**	**5.544**	**0.088**

The optimized step responses of the distributed microgrids are estimated at the same scenario using all 4 objective functions: integral absolute error (IAE), integral square error (ISE), integral time weighted absolute error (ITAE), and integral time weighted square error (ITSE), along with ISWAE and compared in Table 4, for QCSHO tuned PID controllers, which confirmed the superiority of ISWAE over others.

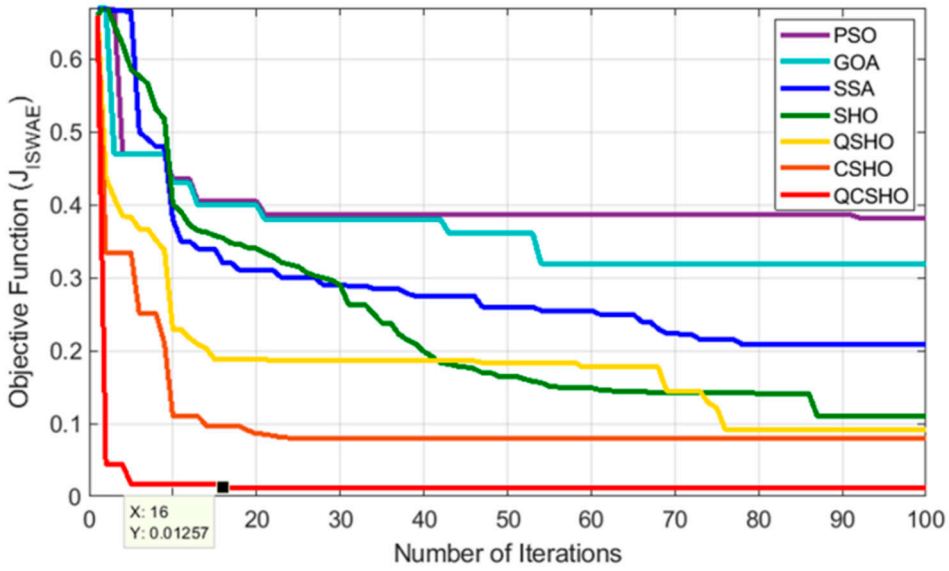

Figure 8. Comparison of the convergence performance for PSO, GOA, SSA, SHO, QSHO, and CSHO with QCSHO.

Table 4. Comparison of controllers using QCSHO and ISWAE.

FOD	I	PI	ID	PD	PID
J_{FOD}	48.515	2801.299	33,576.216	2407.723	**13.205**

The step responses of the distributed microgrids are estimated by separately tuning I, PI, PD, ID, and PID controllers using QCSHO optimized ISWAE and compared in Table 5 estimating J_{FOD}, which confirmed the superiority of PID.

Table 5. Optimized controller gains using QCSHO and ISWAE.

Gains	Interconnected Microgrids		
	Microgrid1	Microgrid2	Microgrid3
K_{Pi1}	9.993	9.985	9.858
K_{Ii1}	10.084	15.142	9.998
K_{Di1}	9.911	10.049	10.147
K_{Pi2}	9.428	9.318	10.064
K_{Ii2}	9.997	10.012	9.942
K_{Di2}	10.500	9.768	10.003
K_{Pi3}	10.009	9.957	17.798
K_{Ii3}	10.230	10.193	10.028
K_{Di3}	10.035	2.742	10.165
L_{DRi}	9.978	10.055	8.237

Finally, the proposed QCSHO algorithm with ISWAE function (J) are preferred for tuning the gains of PID controllers in rest part of the study as these combinations outperform over others, interpreted from Figure 8, Tables 3 and 4 (the superior values are highlighted in bold fonts). The QCSHO tuned PID controller gains for interconnected microgrids are listed in Table 6 considering ISWAE and used in rest of the study without re-tuning PID to investigate the sturdiness of the system.

Table 6. Optimal allocation of DRS and VIS Units.

Cases	Microgrid1		Microgrid2		Microgrid3		J_{FOD}
	VIS	DRS	VIS	DRS	VIS	DRS	
None of SS	0	0	0	0	0	0	4165.7
Only DRS	0	1	0	1	0	1	2528.5
VIS in µG3	0	1	0	1	1	0	3265.6
VIS in µG2	0	1	1	0	0	1	2268.2
VIS in µG2-3	0	1	1	0	1	0	2390.5
VIS in µG1	1	0	0	1	0	1	3566.1
VIS in µG1-3	1	0	0	1	1	0	2363.4
VIS in µG1-2	1	0	1	0	0	1	2662.4
Only VIS	1	0	1	0	1	0	2405.5
Both of SS	1	1	1	1	1	1	1351.8

4.2. Response of Distributed Microgrids

In order to study the system responses round the year in different Indian climatic conditions, the real-time monthly average recorded solar–wind data for Bhubaneswar region [31] and the normalized loading data are arranged with 10 s durations for each month as in Figures 4–6, considering t_{sim} = 120 s. The proposed distributed microgrids, as modelled in Figure 3a, are simulated for simultaneous voltage–frequency regulation in 4 different scenarios of RES penetration with LL as in Figure 5 and one scenario of load variation including NL as in Figure 6 using tuned PID gains from Table 5. The responses for all five cases are plotted and discussed below individually comparing the system responses with both VIS and DRS.

Case 1: Normal Day with Both Solar and Wind Support

This instance is presumed considering a normal day climatic scenario with available RES (SPV, STP, and WTG) generations coordinated with all waste-to-energy-based BEGS (BCHP, MHTG, BGTG, and $BDEG_i$) units including supports from both VIS_i and DRS_i units to supply specified LL ($\Delta P_L = \Delta P_{LL}$). The frequency and voltage responses of the projected distributed microgrids in this scenario are plotted in Figure 9a,b, respectively, along with the tie-line loading in Figure 9c. These confirmed the power quality improvement due to faster support by VIS/DRS units to smoothen Δf_i and Δu_i with minimal ΔP_{tij}. The system voltage, frequency, tie-line loadings are settled to their nominal values within 3, 6, and 1 s, respectively, for every perturbation in source/load as shown in Figure 9a–c. The variation of solar/wind data [31] used for simulation explicitly express the intermittency and the regulated voltage–frequency responses of the system in Case-I scenario confirms the adequacy of control and operation management.

Case 2: Unavailability of Solar Support

This instance is presumed considering a normal night climatic scenario or a cloudy day scenario (or during the maintenance/failure of both SPV and STP units) with WTG generations only to supply the same LL. The waste-to-energy-based BEGS units were coordinated to meet the excess demand in absence of solar support. The frequency, voltage, and tie-line loading responses of the distributed microgrids supported with VIS/DRS in this scenario are plotted in Figure 10a–c, respectively. These also confirmed the power quality improvement with faster settling of Δf_i, Δu_i, and ΔP_{tij} to their nominal values within 2, 5, and 1 s, respectively, for every perturbation in source/load during absence of solar support as shown in Figure 10a–c.

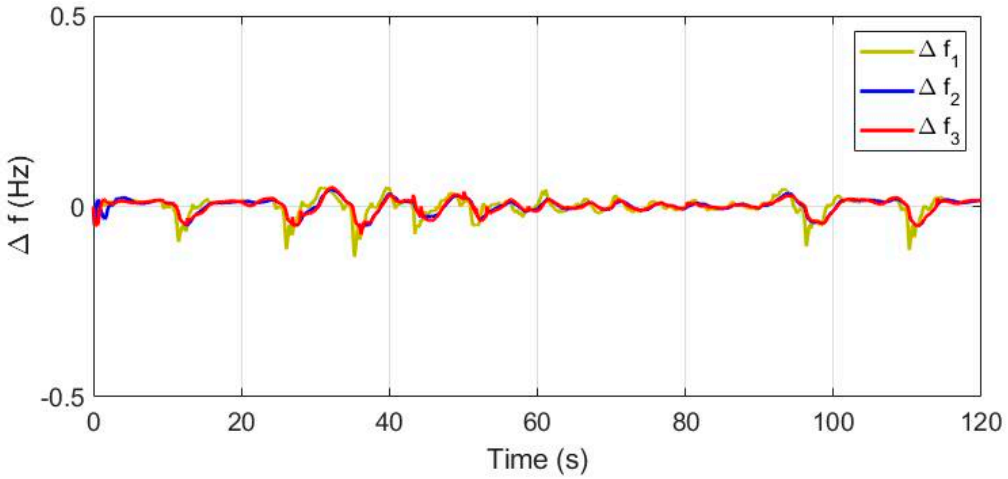

(**a**)

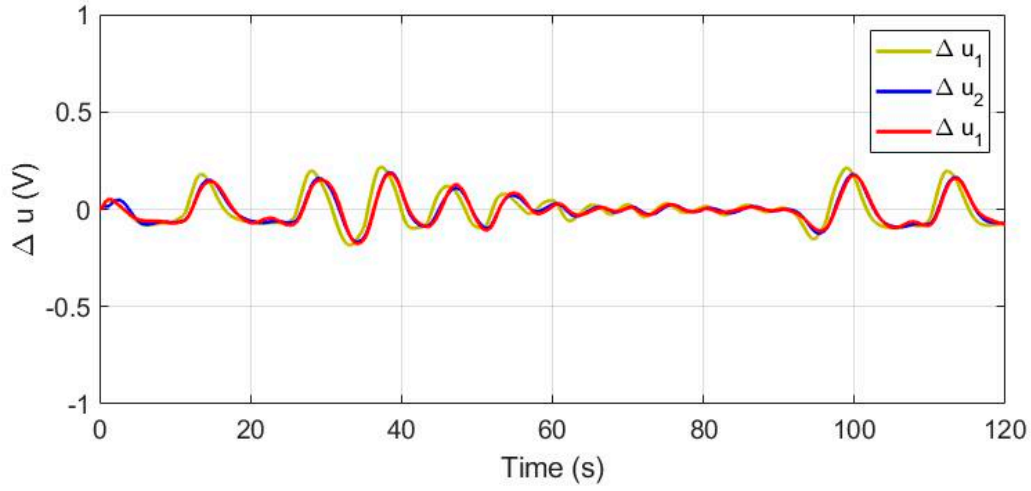

(**b**)

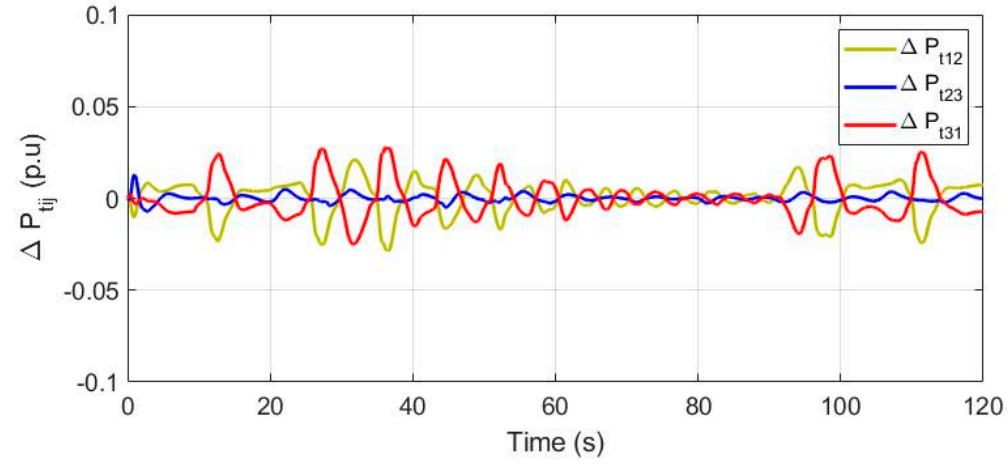

(**c**)

Figure 9. Case 1: (**a**) frequencies (Δf_i), (**b**) voltages (Δu_i), and (**c**) ΔP_{tij} responses.

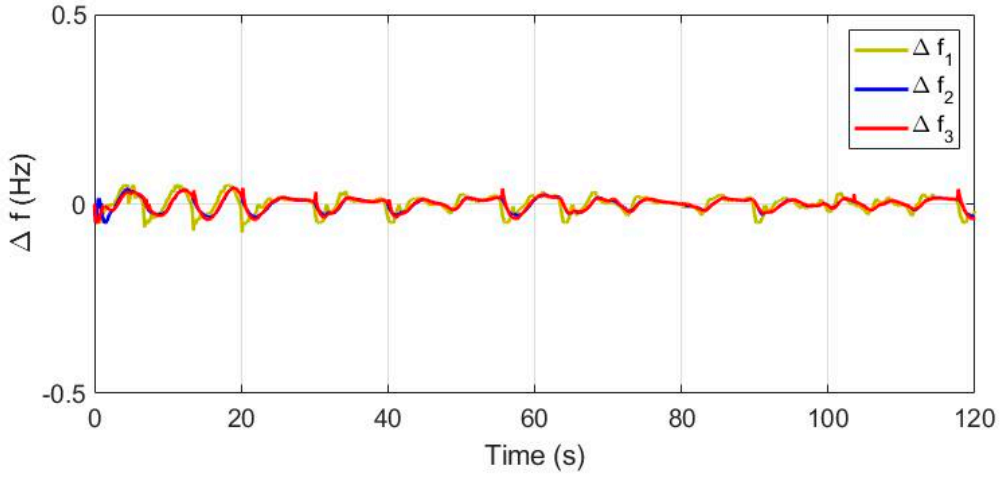

(**a**)

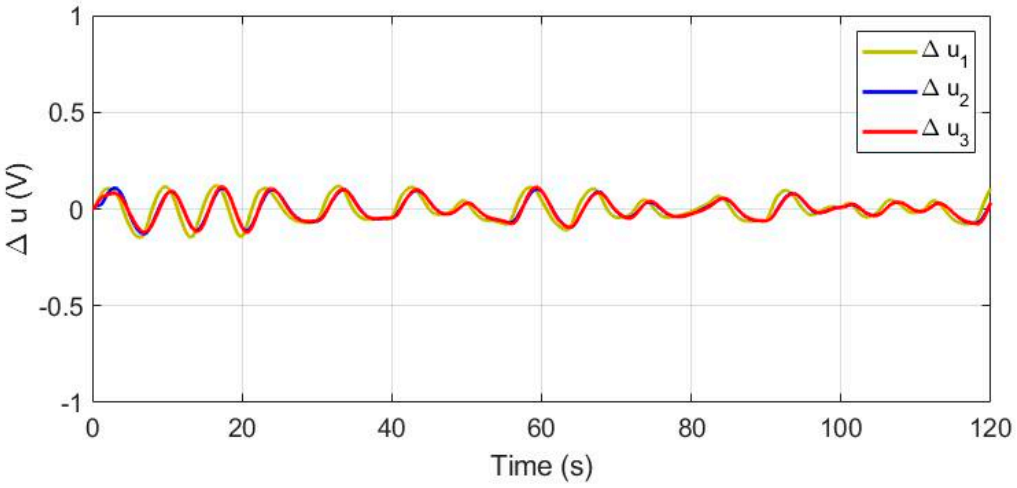

(**b**)

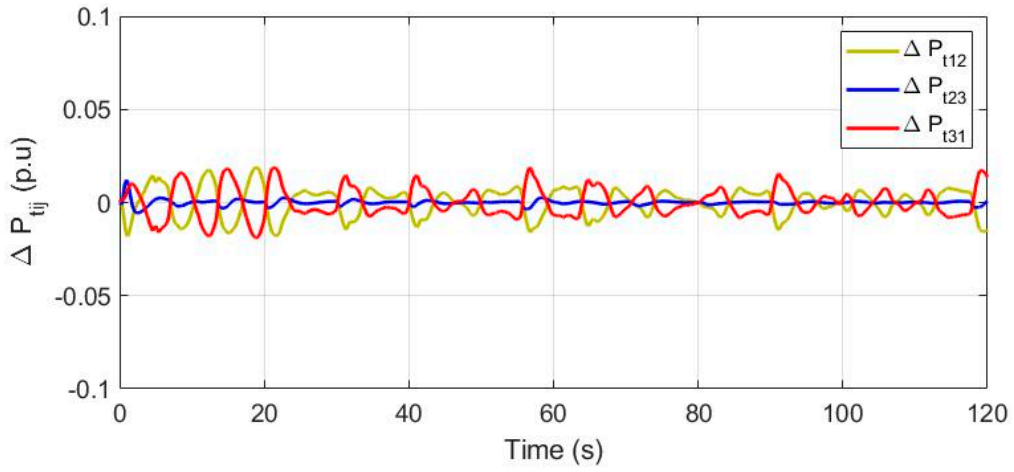

(**c**)

Figure 10. Case 2: (**a**) frequencies (Δf_i), (**b**) voltages (Δu_i), and (**c**) ΔP_{tij} responses.

Case 3: Unavailability of Wind Support

This instance is presumed considering a normal day climatic scenario with unfavorable wind speed (or during the maintenance/failure of WTG unit) with only solar-based RES (i.e., STP and SPV) support to supply that LL. The waste-to-energy-based BEGS units were coordinated to meet the excess demand in absence of wind support.

The frequency, voltage, and tie-line loading responses of the distributed microgrids supported with VIS/DRS in this scenario are plotted in Figure 11a–c, respectively. These confirmed again the power quality improvement with faster settling of Δf_i, Δu_i, and ΔP_{tij} to their nominal values within 2.5, 6, and 1 s, respectively, for every perturbation in source/load during absence of wind support as shown in Figure 11a–c.

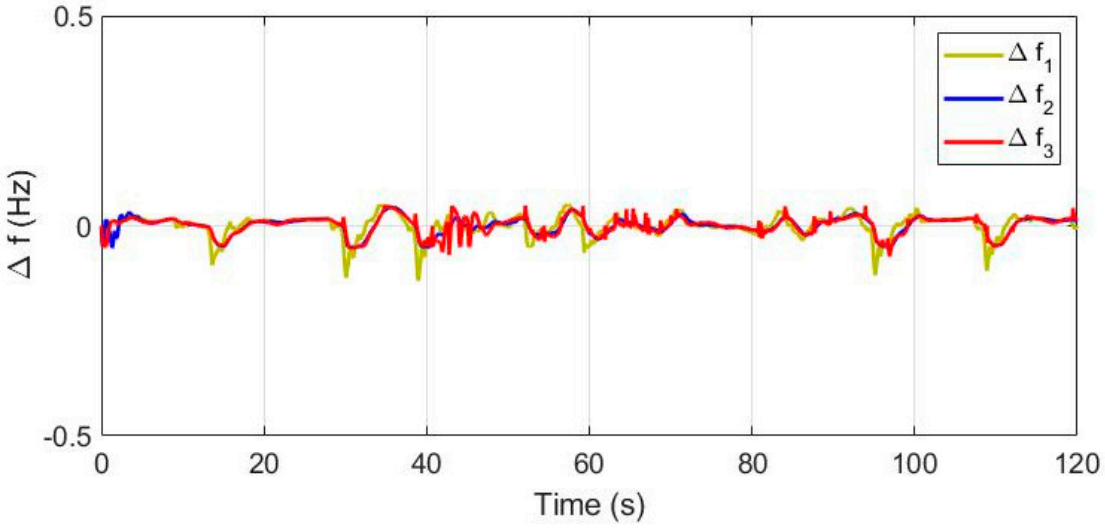

(**a**)

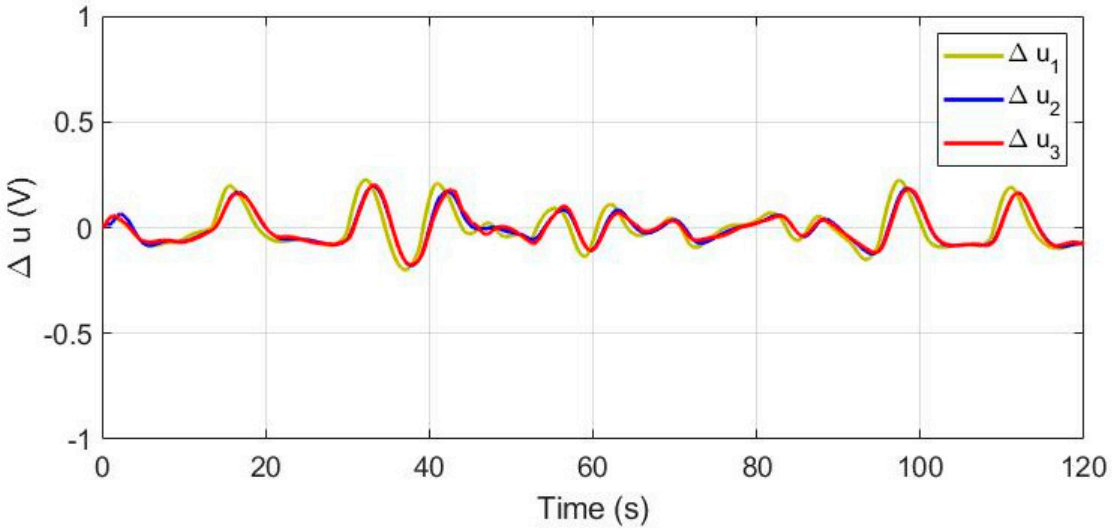

(**b**)

Figure 11. *Cont.*

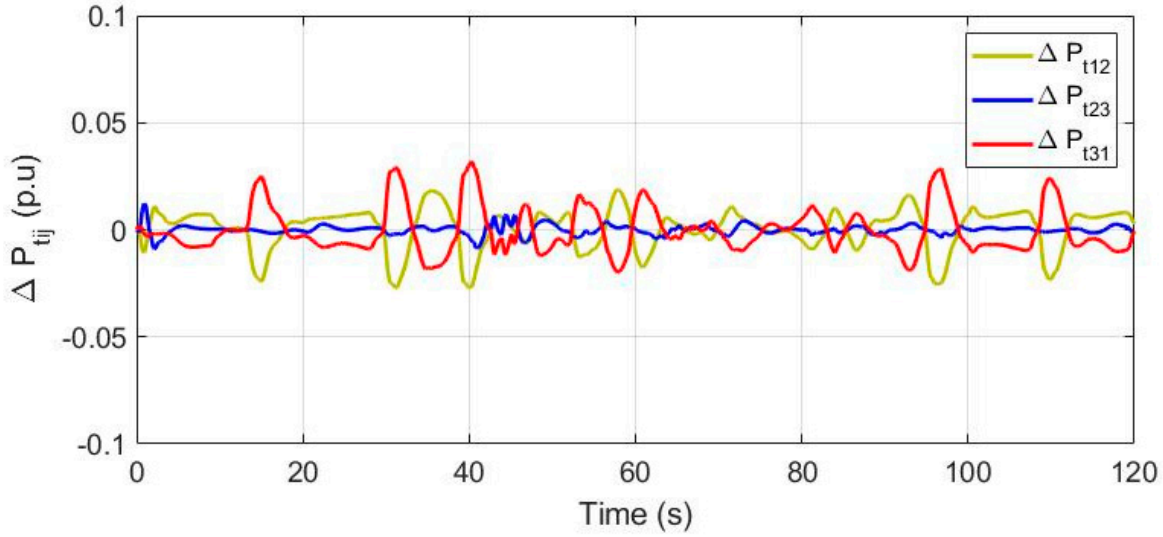

(**c**)

Figure 11. Case 3: (**a**) frequencies (Δf_i), (**b**) voltages (Δu_i), and (**c**) ΔP_{tij} responses.

Case 4: Unavailability of Both Wind and Solar Support

This case is assumed considering a stormy day/night climatic scenario without any RES generations (or maintenance/failure of all RES units) to supply that LL. All the waste-to-energy-based BEGS units were coordinated to meet the total demand in these extreme climatic conditions. The frequency, voltage, and tie-line loading responses of the distributed microgrids supported with VIS/DRS in this scenario are plotted in Figure 12a–c, respectively. These also confirmed the power quality improvement with quicker settling of Δf_i, Δu_i, and ΔP_{tij} to their nominal values within 3, 5, and 1 s, respectively, for every perturbation in source/load during absence of RES support as shown in Figure 12a–c.

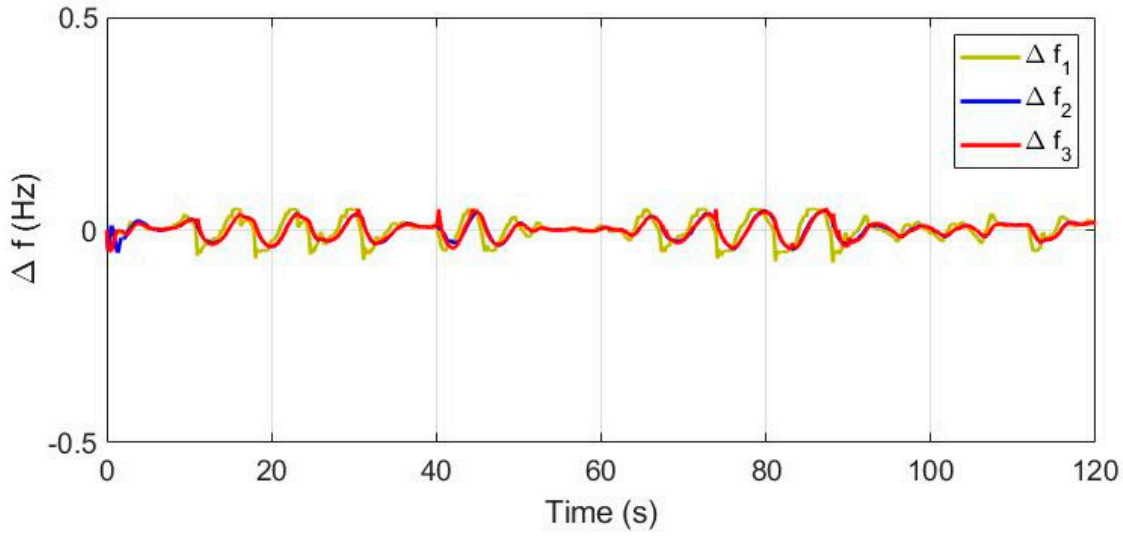

(**a**)

Figure 12. *Cont.*

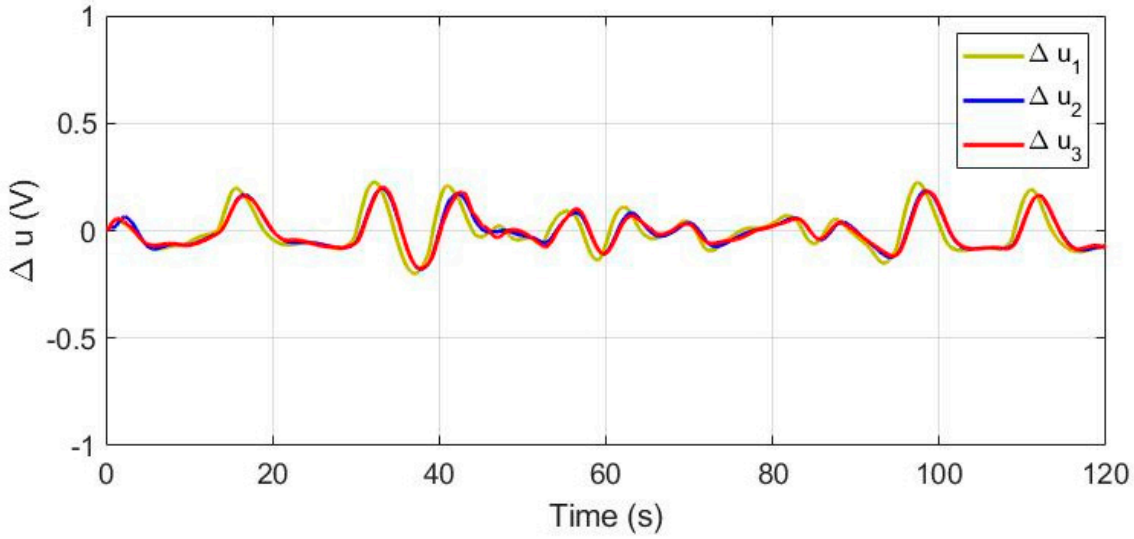

(**b**)

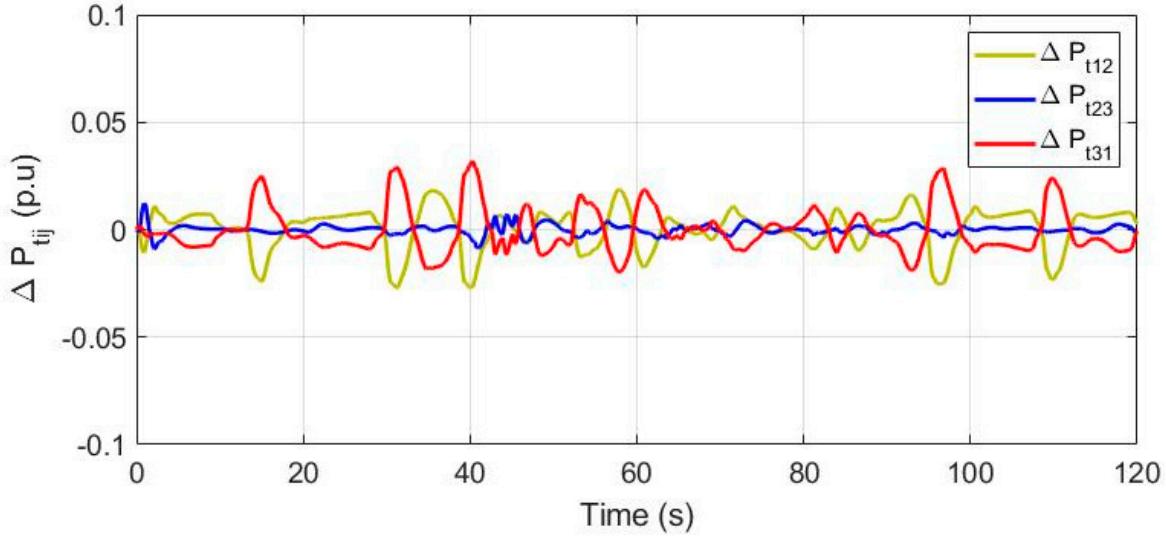

(**c**)

Figure 12. Case 4: (**a**) frequencies (Δf_i), (**b**) voltages (Δu_i), and (**c**) ΔP_{tij} responses.

Case 5: Responses of Distributed Microgrids in Normal Climate with NL

This instance is presumed considering a generalized scenario considering same climatic condition as scenario 1, with all available RES generations supplying combined LL and NL ($\Delta P_L = \Delta P_{LL} + \Delta P_{NL}$). All the waste-to-energy-based BEGS units were coordinated to meet the excess demand. The frequency, voltage, and tie-line loading responses of the projected distributed microgrids supported with VIS/DRS in this generalized loading scenario are plotted in Figure 13a–c, respectively. These are still confirming the power quality improvement with quicker settling of Δf_i, Δu_i, and ΔP_{tij} to their nominal values within 3, 6, and 1 s, respectively, for every perturbation in source/load as shown in Figure 13a–c.

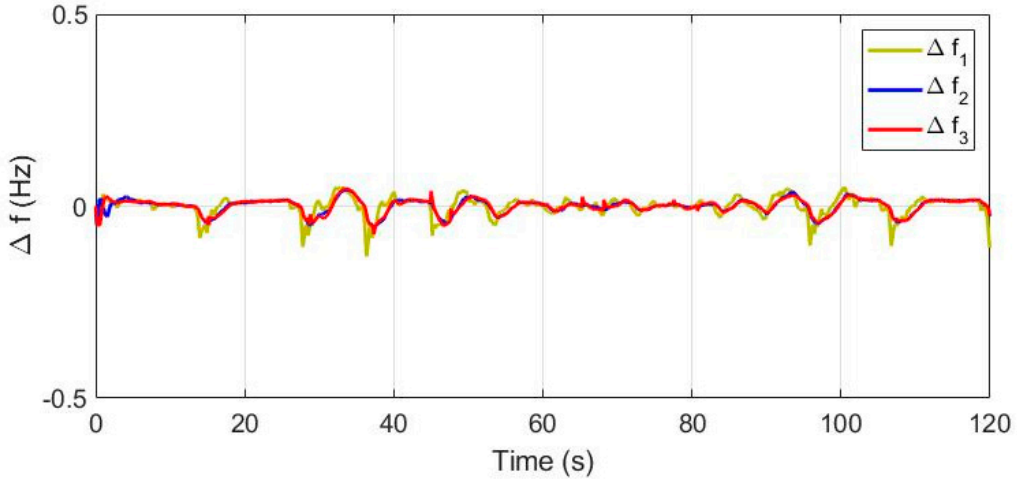

(**a**)

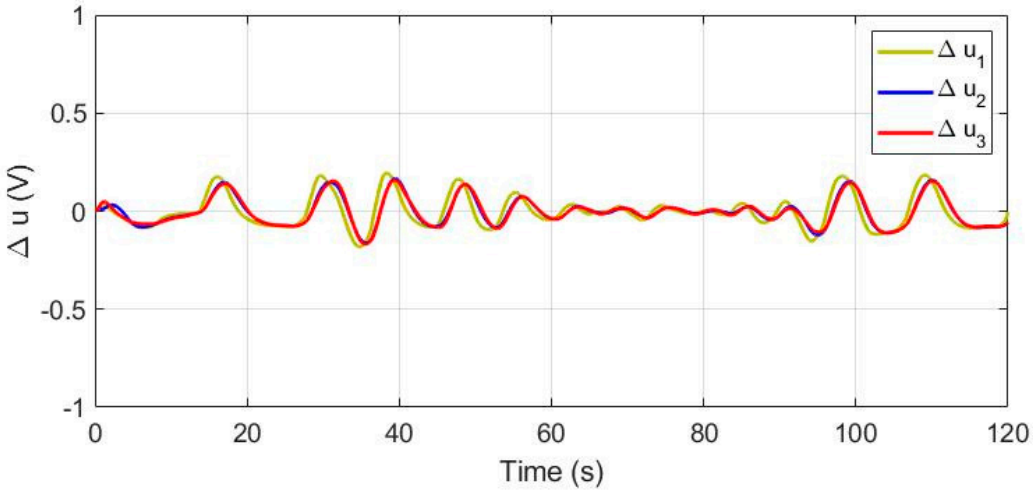

(**b**)

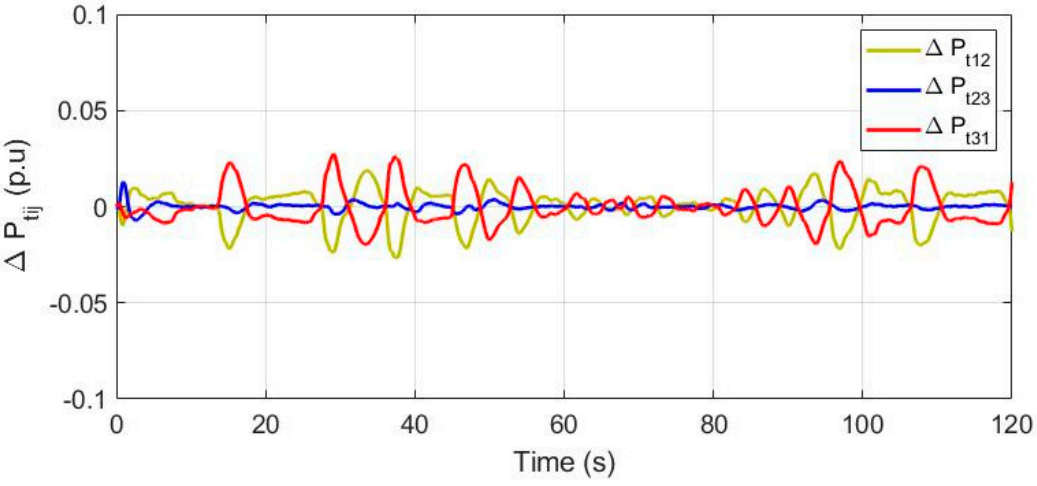

(**c**)

Figure 13. Case 5: (**a**) frequencies (Δf_i), (**b**) voltages (Δu_i), and (**c**) ΔP_{tij} responses.

The responses in all the aforesaid five instances have confirmed robustness of the QCSHO tuned PID controllers and the reliability of projected VIS and DRS units throughout the year, with novel control strategy in distributed microgrids. The work is extended further to investigate the optimal allocation of VIS and DRS units for economic operation of distributed microgrids in next sub-section.

4.3. Optimal Allocation of VIS/DRS Units

The projected distributed microgrids were tested successfully in different extreme climatic/loading scenarios, supported by both VIS and DRS units in each microgrid. However, the arrangement of both VIS and DRS units for each microgrid with suitable control strategies make the system more complex and bulky, which may not be economic (due to additional costs associated with both the support systems). Again, the availability of suitable DR devices and ESS for all these support systems may not be always feasible.

Hence, it is essential to investigate the most suitable arrangements of these VIS and DRS units-based IRP for economic operation of the distributed microgrids. All the 10 possible arrangements of these VIS and DRS units in the distributed microgrids are simulated considering QCSHO tuned PID with ISWAE as listed in Table 6.

The FOD-based performance index (J_{FOD}) was estimated to investigate the optimal allocation of VIS/DRS units for all these 10 cases. The values are compared in Table 6. The optimal system performances could be achieved by allocating both VIS and DRS units to each microgrid, but less economic. Therefore, it is confirmed that installing one VIS unit to hμG2, whereas two DRS units to hμG1 and hμG3 each provide the most economic IRP for the projected distributed microgrids.

All these case studies have confirmed the efficacy and adaptiveness of the proposed QCSHO algorithm for both the modes of operation with quicker coordination by VIS/DRS systems in every climatic variation round the year. Furthermore, suitable monitoring system needs to be implemented in the microgrids for managing the quality of power supply [32]. The acronyms used in this work are listed in Table 7 with their expansions for swift references.

Table 7. List of acronyms.

Acronym	Full Form	Acronym	Full Form
ALFC	Automatic Load Frequency Control	ITSE	Integral of Time-weighted Square Error
AVR	Automatic Voltage Regulator	LFC	Load Frequency Control
BCHP	Biomass-fired Combined Heat and Power	LFR	Linear Fresnel Reflector
BDEG	Bio-Diesel Engine Generator	LL, NL	Linear Loadings, Non-linear Loadings
BEGS	Bio-Energy Generation System	MHTG	Micro-Hydro Turbine Generator
BES	Battery Energy Storage	ORC	Organic Rankine Cycle
BGTG	Bio-Gas Turbine Generator	PD	Proportional-Derivative
CES	Capacitive Energy Storage	PI	Proportional-Integral
CLS	Chaotic Linear Search	PID	Proportional-Integral-Derivative
CSHO	Chaotic Selfish-Herd Optimization	PSO	Particle Swarm Optimization
DRS	Demand Response Support	PTC	Parabolic Trough Collector
DSM	Demand Side Management	QCSHO	Quasi-oppositional Chaotic Selfish Herd Optimization
ESS	Energy Storage System	QOBL	Quasi Opposition-Based Learning
FOD	Figures Of Demerits	RES	Renewable Energy System
GOA	Grasshopper Optimization Algorithm	SHO	Selfish Herd Optimization

Table 7. *Cont.*

Acronym	Full Form	Acronym	Full Form
HEV	Hybrid Electric Vehicles	SPV	Solar Photovoltaic
I	Integral	SOC	Sate Of Charge
IAE	Integral Absolute Error	SSA	Salp Swarm Algorithm
ID	Integral-Derivative	SSM	Supply Side Management
IRP	Integrated Resource Planning	STP	Solar Thermal Power
ISE	Integral Square Error	VIS	Virtual Inertia Support
ISWAE	Integral Square of Weighted Absolute Error	WTG	Wind Turbine Generator
ITAE	Integral of Time-weighted Absolute Error		

5. Conclusions

The results obtained in this study have collectively confirmed the performance improvement of distributed microgrids, incorporating the proposed VIS/DRS system. The system performances using new QCSHO tuned PID controllers considering ISWAE were found superior to expedite optimal voltage, frequency, and tie-line loadings within accessible operating limits. Again, the overall system responses supported with both VIS and DRS units have witnessed adaptive throughout the year, with 5 different scenarios of extreme climatic and load variations. The smooth regulation and faster settling of voltage and frequency in all these five scenarios (without re-tuning the controller gains) confirmed the sturdiness of the proposed system. The study is extended further for optimal allocation of these VIS/DRS units in the projected microgrids estimating FOD-based performance index in 10 possible arrangements. Finally, the system responses have confirmed the economic IRP by incorporating the proposed VIS in the second microgrid only and 2 DRS units in other two microgrids for optimal allocation. This work could be extended further with modern controllers such as model-predictive, fractional-order, fuzzy, their blends along with available standard technique for tuning the control parameters, and comparative performance study.

Author Contributions: Conceptualization, A.K.B., A.L. and D.C.D.; methodology, A.K.B.; software, A.K.B.; validation, A.K.B. and D.C.D.; formal analysis, A.K.B., A.L., S.M.S.H. and T.S.U.; investigation, A.K.B.; resources, A.K.B.; data curation, A.K.B.; writing—original draft preparation, A.K.B.; writing—review and editing, A.K.B., D.C.D., A.L., S.M.S.H. and T.S.U.; visualization, A.K.B.; supervision, D.C.D.; project administration, S.M.S.H. and T.S.U.; funding acquisition, S.M.S.H. and T.S.U. All authors have read and agreed to the published version of the manuscript.

Funding: This research received no external funding.

Institutional Review Board Statement: Not applicable.

Informed Consent Statement: Not applicable.

Data Availability Statement: Not applicable.

Conflicts of Interest: The authors declare no conflict of interest.

References

1. Barik, A.K.; Das, D.C. Coordinated regulation of Voltage and Load-Frequency in Demand response supported Bio-renewable cogeneration based Isolated hybrid Microgrid with Quasi-oppositional Selfish Herd Optimisation. *Int. Trans. Electr. Energy Syst.* **2020**, *30*, 1–22. [CrossRef]
2. Zou, H.; Mao, S.; Wang, Y.; Zhang, F.; Chen, X.; Cheng, L. A survey of energy management in interconnected multi-microgrids. *IEEE Access* **2019**, *7*, 72158–72169. [CrossRef]
3. Bevrani, H.; Ise, T.; Miura, Y.; Watanabe, M. Virtual synchronous generators: A survey and new perspectives. *Int. J. Electr. Power Energy Syst.* **2014**, *54*, 244–254. [CrossRef]
4. Yang, L.; Hu, Z.; Xie, S.; Kong, S.; Lin, W. Adjustable virtual inertia control of supercapacitors in PV-based AC microgrid cluster. *Electr. Power Syst. Res.* **2019**, *73*, 71–85. [CrossRef]

5. Kerdphol, T.; Rahman, F.S. Robust virtual inertia control of a low inertia microgrid considering frequency measurement effects. *IEEE Access* **2019**, *7*, 57550–57560. [CrossRef]
6. Fini, M.H.; Golshan, M.E.H. Determining optimal virtual inertia and frequency control parameters to preserve the frequency stability in islanded microgrids with high penetration of renewables. *Electr. Power Syst. Res.* **2018**, *154*, 13–22. [CrossRef]
7. Kerdphol, T.; Watanabe, M.; Mitani, Y.; Phunpeng, V. Applying Virtual Inertia Control Topology to SMES System for Frequency Stability Improvement of Low-Inertia Microgrids Driven by High Renewables. *Energies* **2019**, *12*, 3902. [CrossRef]
8. Shintai, T.; Miura, Y.; Ise, T. Oscillation damping of a distributed generator using a virtual synchronous generator. *IEEE Trans. Power Deliv.* **2014**, *29*, 668–676. [CrossRef]
9. Fathi, A.; Shafiee, Q.; Bevrani, H. Robust frequency control of microgrids using an extended virtual synchronous generator. *IEEE Trans. Power Syst.* **2018**, *33*, 6289–6297. [CrossRef]
10. Phurailatpam, C.; Rather, Z.H.; Bahrani, B.; Doolla, S. Measurement Based Estimation of Inertia in AC Microgrids. *IEEE Trans. Sustain. Energy* **2020**, *11*, 1975–1985. [CrossRef]
11. Barik, A.K.; Jaiswal, S.; Das, D.C. Recent trends and development in hybrid microgrid: A review on energy resource planning and control. *Int. J. Sustain. Energy* **2021**, 1–15. [CrossRef]
12. Bao, Y.Q.; Li, Y.; Wang, B.; Hong, Y.-Y. Design of a hybrid hierarchical demand response control scheme for the frequency control. *IET Gener. Transm. Distrib.* **2015**, *9*, 2303–2310. [CrossRef]
13. Bao, Y.Q.; Li, Y.; Wang, B.; Hu, M.; Chen, P. Demand response for frequency control of multi-area power system. *J. Mod. Power Syst. Clean Energy* **2017**, *5*, 20–29. [CrossRef]
14. Zakariazadeh, A.; Homaee, O.; Jadid, S.; Siano, P. A new approach for real time voltage control using demand response in an automated distribution system. *Appl. Energy* **2014**, *117*, 157–166. [CrossRef]
15. Pourmousavi, S.A.; Nehrir, M.H. Real-time central demand response for primary frequency regulation in microgrids. *IEEE Trans. Smart Grid* **2012**, *3*, 1988–1996. [CrossRef]
16. Ly, A.; Bashash, S. Fast Transactive Control for Frequency Regulation in Smart Grids with Demand Response and Energy Storage. *Energies* **2020**, *13*, 4771. [CrossRef]
17. Barik, A.K.; Das, D.C. Proficient Load-frequency regulation of demand response supported Bio-renewable cogeneration based hybrid Microgrids with Quasi-oppositional Selfish-herd Optimisation. *IET Gener. Transm. Distrib.* **2019**, *13*, 2889–2898. [CrossRef]
18. Barik, A.K.; Das, D.C.; Muduli, R. Demand Response Supported Optimal Load-Frequency Regulation of Sustainable Energy based Four-Interconnected Unequal Hybrid Microgrids. In Proceedings of the IEEE International Conference on Sustainable Energy Technologies and Systems (ICSETS), Bhubaneswar, India, 26 February–1 March 2019.
19. Othman, A.M.; El-Fergany, A.A. Design of robust model predictive controllers for frequency and voltage loops of interconnected power systems including wind farm and energy storage system. *IET Gener. Transm. Distrib.* **2018**, *12*, 4276–4283. [CrossRef]
20. Barik, A.K.; Das, D.C. Expeditious frequency control of solar photovoltaic/biogas/biodiesel generator based isolated renewable microgrid using grasshopper optimisation algorithm. *IET Renew. Power Gener.* **2018**, *12*, 1659–1667. [CrossRef]
21. Bhuyan, M.; Barik, A.K.; Das, D.C. GOA optimized frequency control of Solar Thermal/Sea-Wave/Biodiesel Generator based interconnected hybrid microgrids with DC link. *Int. J. Sustain. Energy* **2020**, *39*, 615–633. [CrossRef]
22. Barik, A.K.; Tripathy, D.; Das, D.C.; Sahoo, S.C. Optimal Load-frequency regulation of Demand response supported Isolated Hybrid Microgrid using Fuzzy PD+I Controller. In Proceedings of the International Conference on Innovation in Modern Science and Technology, Siliguri, India, 20–21 September 2019; Springer International Publishing: Berlin/Heidelberg, Germany, 2020; Volume 12, pp. 798–806.
23. Latif, A.; Das, D.C.; Barik, A.K.; Ranjan, S. Illustration of demand response supported coordinated system performance evaluation of YSGA optimized dual stage PIFOD-(1+PI) controller employed with wind-tidal-biodiesel based independent two-area interconnected microgrid system. *IET Renew. Power Gener.* **2020**, *14*, 1074–1086. [CrossRef]
24. Latif, A.; Hussain, S.M.; Das, D.C.; Ustun, T.S. Optimum Synthesis of a BOA optimized novel dual-stage PI-(1+ID) controller for frequency response of a microgrid. *Energies* **2020**, *13*, 3446. [CrossRef]
25. Barik, A.K.; Das, D.C. Active power management of isolated renewable microgrid generating power from Rooftop solar arrays, sewage waters and solid urban wastes of a smart city using Salp swarm algorithm. In Proceedings of the International Conference on Technologies for Smart-City Energy Security and Power (ICSESP), Bhubaneswar, India, 28–30 March 2018.
26. Barik, A.K.; Das, D.C. A storage based Virtual Synchronous System for Load-frequency regulation of interconnected Hybrid Microgrids using Selfish-herd optimiser. In Proceedings of the International Conference on Renewable Energy Integration into Smart Grids (ICREISG), Bhubaneswar, India, 14–15 February 2020.
27. Saha, S.; Mukherjee, V. A novel quasi-oppositional chaotic antlion optimizer for global optimization. *Appl. Intell.* **2018**, *48*, 2628–2660. [CrossRef]
28. Fausto, F.; Cuevas, E.; Valdivia, A.; González, A. A global optimization algorithm inspired in the behavior of selfish herds. *Biosystems* **2017**, *160*, 39–55. [CrossRef] [PubMed]
29. Kundur, P. *Power System Stability and Control*, reprint ed.; Balu, N., Lauby, M.G., Eds.; McGraw-Hill: New York, NY, USA, 2009; pp. 309–366.
30. Lee, D.J.; Wang, L. Small-signal stability analysis of an autonomous hybrid renewable energy power generation/energy storage system part I: Time-domain simulations. *IEEE Trans. Energy Convers.* **2008**, *23*, 311–320. [CrossRef]

31. NASA Surface Meteorology and Solar Energy. Available online: https://power.larc.nasa.gov/ (accessed on 2 April 2021).
32. Barik, A.K.; Tripathy, D.; Mohanty, A.K. Detection & Mitigation of Power Quality Disturbances using WPT & FACTS Technology. *Int. J. Sci. Eng. Technol. Res.* **2013**, *2*, 336–343.